Geotail observations of magnetic flux ropes in the plasma sheet

J. A. Slavin,[1] R. P. Lepping,[1] J. Gjerloev,[1] D. H. Fairfield,[1] M. Hesse,[1] C. J. Owen,[2] M. B. Moldwin,[3] T. Nagai,[4] A. Ieda,[5] and T. Mukai[5]

Received 24 June 2002; revised 22 September 2002; accepted 2 October 2002; published 11 January 2003.

[1] Examination of Geotail measurements in the near-tail ($X > -30\ R_E$) has revealed the presence of small flux ropes in the plasma sheet. A total of 73 flux rope events were identified in the Geotail magnetic field measurements between November 1998 and April 1999. This corresponds to an estimated occurrence frequency of ~1 flux rope per 5 hours of central plasma sheet observing time. All of the flux ropes were embedded within high-speed plasma sheet flows with 35 directed Earthward, $\langle V_x \rangle = 431$ km/s, and 38 moving tailward, $\langle V_x \rangle = -451$ km/s. We refer to these two populations as "BBF-type" and "plasmoid-type" flux ropes. The flux ropes were usually several tens of seconds in duration, and the two types were readily distinguished by the sense of their quasisinusoidal ΔB_z perturbations, i.e., $\mp$ for the "BBF" events and $\pm$ for the "plasmoid" events. Most typically, a flux rope was observed to closely follow the onset of a high-speed flow within ~1–2 min. Application of the Lepping-Burlaga constant-α flux rope model (i.e., $\mathbf{J} = \alpha\mathbf{B}$) to these events showed that approximately 60% of each class could be acceptably described as cylindrical, force-free flux ropes. The modeling results yielded mean flux rope diameters and core field intensities of 1.4 R_E and 20 nT and 4.4 R_E and 14 nT for the BBF and plasmoid-type events, respectively. The inclinations of the flux ropes were small relative to the GSM X–Y plane, but a wide range of azimuthal orientations were determined within that plane. The frequent presence of these flux ropes in the plasma sheet is interpreted as strong evidence for multiple reconnection X-lines (MRX) in the near-tail. Hence, our results suggest that reconnection in the near-tail may closely resemble that at the dayside magnetopause where MRX reconnection has been hypothesized to be responsible for the generation of flux transfer events. *INDEX TERMS:* 2740 Magnetospheric Physics: Magnetospheric configuration and dynamics; 2764 Magnetospheric Physics: Plasma sheet; 2744 Magnetospheric Physics: Magnetotail; 2788 Magnetospheric Physics: Storms and substorms

Citation: Slavin, J. A., R. P. Lepping, J. Gjerloev, D. H. Fairfield, M. Hesse, C. J. Owen, M. B. Moldwin, T. Nagai, A. Ieda, and T. Mukai, Geotail observations of magnetic flux ropes in the plasma sheet, *J. Geophys. Res.*, *108*(A1), 1015, doi:10.1029/2002JA009557, 2003.

1. Introduction

[2] The ISEE 1 & 2 and AMPTE IRM measurements [*Baumjohann et al.*, 1990; *Angelopolous et al.*, 1992] provided direct confirmation of the correlated high-speed Earthward/tailward flows and northward/southward magnetic fields in the near-Earth plasma sheet predicted by *Dungey*'s [1961] theory of reconnection-driven magnetospheric convection. Our understanding of these high-speed plasma flows was then greatly expanded by the Geotail mission [*Mukai et al.*, 1996]. In particular, the mean distance to the near-Earth neutral line (NENL) at substorm onset has been determined to be $X \sim -25\ R_E$ [*Nagai et al.*, 1998a] and direct measurements in the vicinity of active neutral lines were returned [*Hoshino*, 1998; *Nagai et al.*, 2001]. The flows out of neutral lines are predicted and observed to have speeds comparable to the Alfven speed in the in-flow region. Hence, the term "Alfvenic jet" is often used to describe the high-speed flows Earthward and tailward of reconnection neutral lines. Indeed, Geotail has measured flows in the central plasma sheet with magnitudes exceeding 2000 km/s [*Fairfield et al.*, 1998]. Finally, a persistent "distant neutral line" (DNL) was observed by ISEE 3 and Geotail at a mean downstream distance of $X \sim -100\ R_E$ [*Slavin et al.*, 1985; *Nishida et al.*, 1994, 1998]. Beyond this distance the plasma sheet flow is nearly always tailward at a few hundred to a thousand km/s.

[3] *Schindler* [1974] and *Hones* [1977] developed theories regarding the macroscopic effects of reconnection upon the magnetic topology of the tail. In particular, they differ-

[1]Laboratory for Extraterrestrial Physics, National Aeronautics and Space Administration/Goddard Space Flight Center, Greenbelt, Maryland, USA.
[2]Mullard Space Science Laboratory, University College London, Dorking, UK.
[3]ESS/Institute of Geophysics and Planetary Physics, University of California at Los Angeles, Los Angeles, California, USA.
[4]Department of Earth and Planetary Sciences, Tokyo Institute of Technology, Tokyo, Japan.
[5]Institute of Space and Astronautical Science, Sagamihara, Japan.

0148-0227/03/2002JA009557$09.00

entiated between the effects of a reconnection involving the "closed" magnetic field lines constituting the plasma sheet as opposed to the open flux comprising the lobes. In two dimensions, the formation of one or more *X*-lines on closed field lines always leads to the formation of magnetic loops or "islands" [*Schindler*, 1974]. Similarly, reconnection at a single *X*-line involving the oppositely directed, lobe field lines creates "closed" and "interplanetary" field lines on the Earthward and tailward sides of the neutral line, respectively. *Hones* [1977] first proposed a sequence of events by which closed field line reconnection in the plasma sheet is followed by open flux reconnection to produce substorms. Most notably, he predicted the formation of closed loops of magnetic flux between the near and distant neutral lines which he termed "plasmoids". They are then driven tailward at high speed by the pressure gradients and the tension in the newly created interplanetary field lines generated by the subsequent reconnection of lobe flux at the NENL.

[4] Plasmoids resembling those predicted by *Schindler* [1974] and *Hones* [1977] were observed in the mid-1980's by ISEE 3 [*Hones et al.*, 1984; *Baker et al.*, 1987; *Richardson et al.*, 1987; *Slavin et al.*, 1989; *Moldwin and Hughes*, 1992]. Intensive investigation was then undertaken using the more comprehensive instrumentation carried by Geotail [*Nagai et al.*, 1994, 1998a, 1998b; *Mukai et al.*, 1996, 1998; *Ieda et al.*, 1998, 2001; *Slavin et al.*, 1998, 1999, 2002; *Machida et al.*, 2000]. In particular, the Geotail observations showed that the plasmoids are far more dynamic than suggested by the ISEE 3 data with small, $< 10\ R_E$, plasmoids being formed in the near-tail, $X \sim -25$ to $-50\ R_E$, and then growing in size and downtail speed until they reach lengths of several tens of Earth radii by $X \sim -100\ R_E$ [*Ieda et al.*, 1998, 2001; *Slavin et al.*, 1998, 1999].

[5] The 2-D magnetic loop topologies considered by Schindler and Hones are, of course, not achievable in 3-D because perfect alignment of the oppositely directed magnetic field lines would be required. Indeed, the stresses exerted at the magnetopause by reconnection act to shear the two lobes and impress a small B_y throughout the magnetosphere [*Cowley*, 1981]. *Hughes and Sibeck* [1987], *Birn et al.* [1989], and *Moldwin and Hughes* [1991] demonstrated that this small B_y in the plasma sheet leads naturally to the generation of magnetic "flux ropes" as opposed to "loops" when reconnection takes place. Although the magnetic fields within plasmoids are often irregular and complex [e.g., *Slavin et al.*, 1989], they have a clear tendency toward helical magnetic field topologies [*Moldwin and Hughes*, 1992; *Lepping et al.*, 1995; *Slavin et al.*, 1995; *Ieda et al.*, 1998]. In this study we will term any magnetic flux rope transported tailward as being of the "plasmoid-type".

[6] Figure 1 provides a schematic depiction of the variation of magnetic field line geometry as a function of distance from the center of the flux rope [e.g., *Priest*, 1990; *Lepping et al.*, 1990]. Along the central axis of the flux rope the magnetic field, $\mathbf{B_o}$, is most intense, and parallel to the central axis, i.e., **z**. For a cylindrical flux rope there is no radial magnetic field, i.e., $\mathbf{B_r} = 0$. As one moves outward from the central axis the B_z magnetic field weakens while the azimuthal magnetic field, $\mathbf{B}_\theta$, becomes stronger. The electric current (not shown) can be either parallel or antiparallel to the sense of the magnetic field lines in the flux rope. When IMF B_y is positive (i.e., away sectors), the B_y in the tail will also tend to be positive and the current density vector in any flux ropes created under these conditions will be parallel to the magnetic field or "right-handed" [e.g., *Lepping et al.*, 1990]. Conversely, "left-handed" flux ropes with the current and magnetic field being antiparallel are expected when IMF B_y and B_y in the tail are negative (i.e., toward sectors).

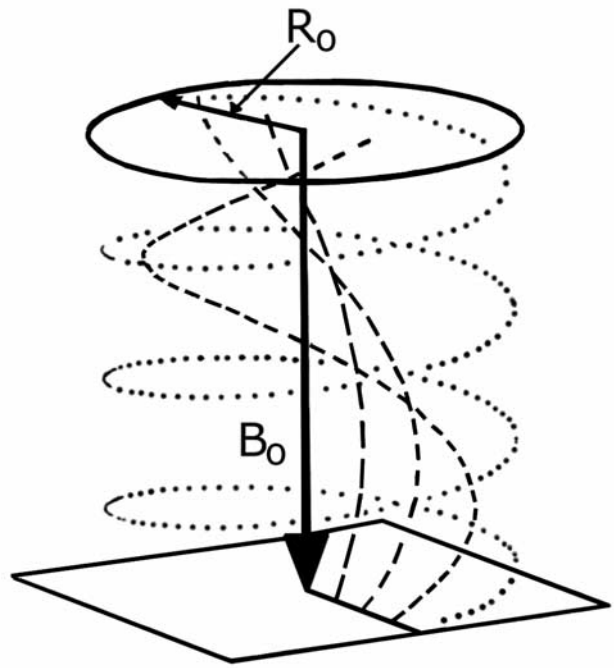

Figure 1. Schematic depiction of a magnetic flux rope of radius, R_o, and core magnetic field, B_o. Long-dash, short-dash and dotted lines indicate field lines emanating from increasing distances from the central axis of the flux rope. In the cylindrical coordinates used in equation (1), the *z* axis is directed upward along the axis of the flux rope, r is positive outward from the central axis, and θ is measured about the *z* axis positive in a right-handed sense.

[7] The stress equilibrium for a cylindrical flux rope [*Priest*, 1990] is given by:

$$dP/dr + d/dr\left(B_\theta^2 + B_z^2\right)/2\mu + B_\theta^2/\mu = 0 \qquad (1)$$

where P is the thermal pressure of the plasma. Accordingly, it is expected that the change in the magnitude of the field and the "pitch angle" of the lines of force are directly related to the nature of the plasma pressure gradient outward from the central axis of the flux rope. However, there is a special class of flux ropes characterized by relatively small pressure gradients, $dP/dr \sim 0$. Within these flux ropes the high outward magnetic pressures exerted by the strong axially aligned magnetic fields in the core region are balanced mainly by the inward magnetic tension of the small pitch angle field lines in the outer layers of the flux rope. These self-balancing flux ropes are generally referred to as being "force-free" due to their small internal pressure gradients and $\mathbf{J} \times \mathbf{B}$ forces. Force-free flux ropes are of special interest for cosmic plasmas because they correspond

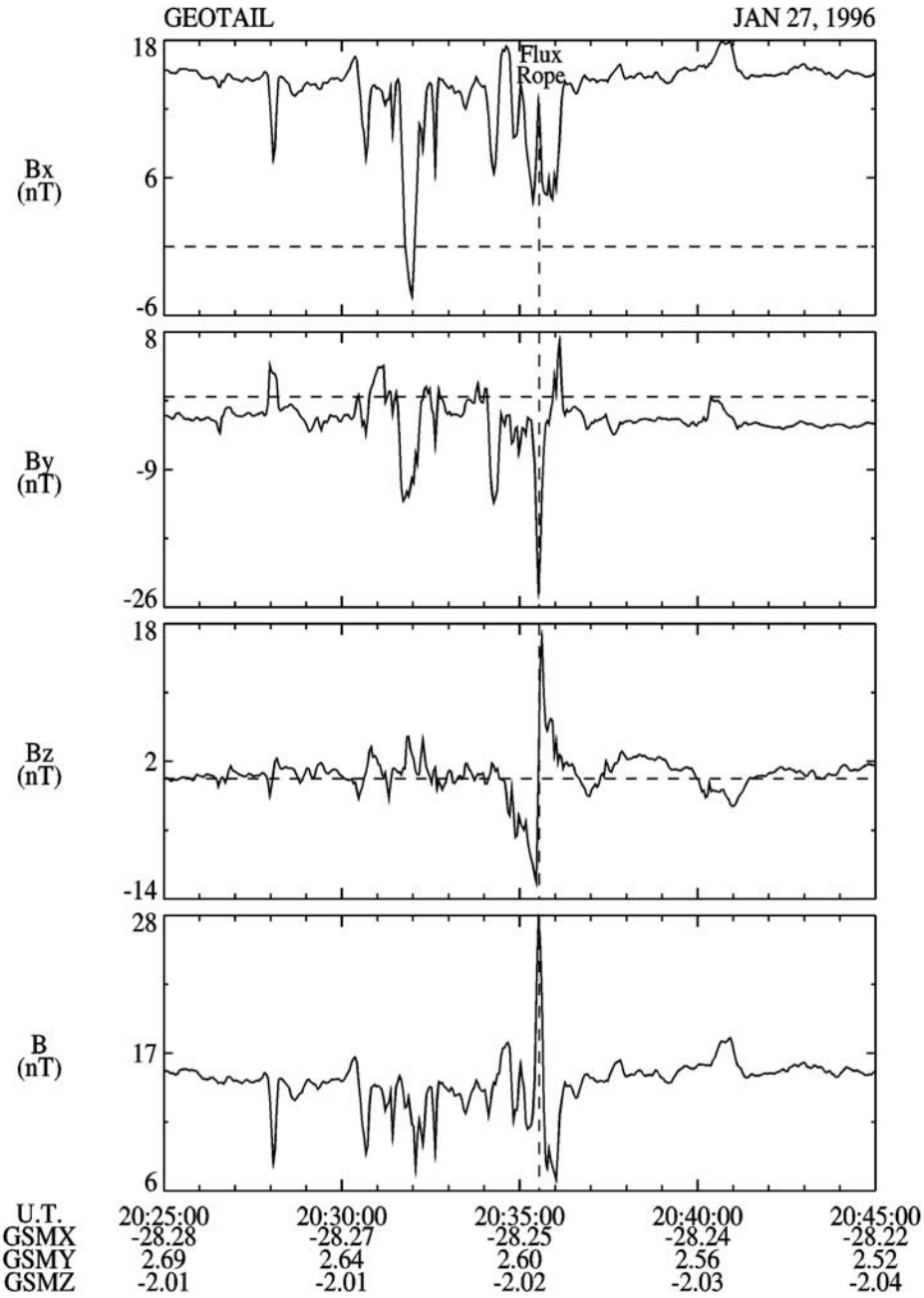

Figure 2a. An example of Geotail magnetic field observations of a flux rope event on 27 January 1996. Note the very strong "core" B_y magnetic field enhancement coincident with the south-then-north B_z variation.

to the minimum energy state for helical magnetic fields and, hence, may represent end points for the evolution of these structures [*Priest*, 1990]. Such force-free flux rope field configurations have been observed in the core regions of plasmoids in the distant tail and successfully modeled by *Moldwin and Hughes* [1991], *Lepping et al.* [1995, 1996], and *Slavin et al.* [1995]. A review of distant tail plasmoid-type flux ropes and issues relating to their formation may be found in the work of *Hesse and Kivelson* [1998].

[8] In addition to the plasmoids, there have been some reports of individual flux ropes being transported Earthward in the ISEE 1, 2 & 3, IMP 8 and the Galileo Earth flyby measurements [*Elphic et al.*, 1986; *Moldwin and Hughes*, 1992; *Sergeev et al.*, 1992; *Kivelson et al.*, 1993; *Moldwin and Hughes*, 1994; *Khurana et al.*, 1995]. Again, good success was achieved modeling these flux ropes as force-free structures. For the purposes of this study we will term all flux ropes transported Earthward as being "BBF-type" flux ropes due to the close association between them and bursty bulk flows that will be demonstrated in this paper.

[9] In this article we report upon the first survey of Earthward moving flux ropes in the near-tail plasma sheet at distances of $X > -30\ R_E$ using the Geotail measurements. Although special emphasis will be placed upon the less well

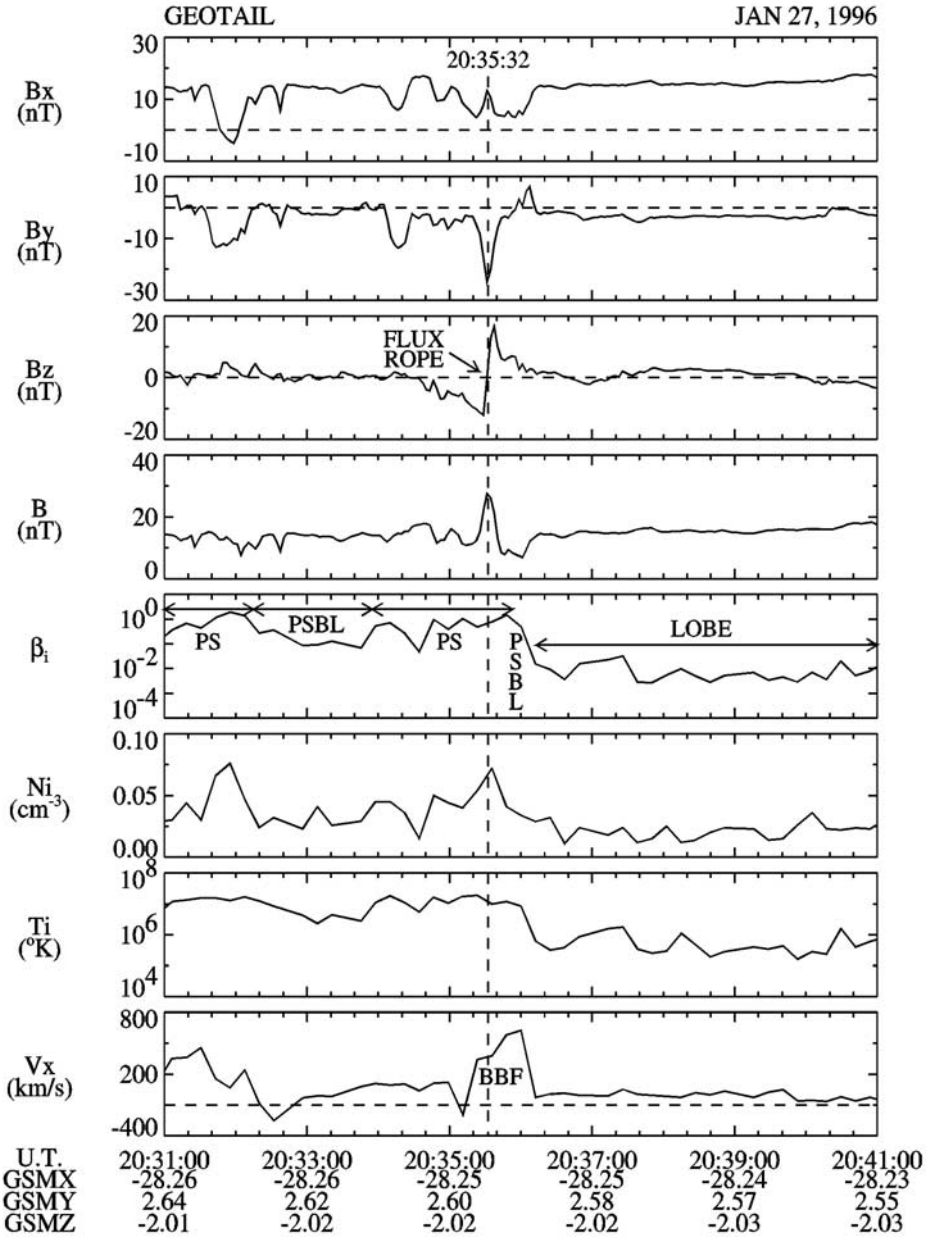

Figure 2b. Geotail plasma measurements during the flux rope event on 27 January 1996. As shown, the flux rope was embedded within the plasma sheet (i.e., $\beta \sim 0.5-0.7$).

examined BBF-type flux ropes, we will also, for comparative purposes, identify tailward moving flux ropes and present a parallel analysis of those events. Using the plasma and magnetic field measurements returned by the Geotail Mission, we will show that flux ropes are a common occurrence in the near-Earth plasma sheet and that they are closely associated with fast Earthward and tailward flows. On this basis we will argue that the onset of reconnection involves a large section of the cross-tail current layer with a region perhaps $\sim 10\ R_E$ in length along the Sun–Earth line becoming unstable and leading to closed field line reconnection at multiple *X*-lines and the consequent formation of flux ropes. However, the process must quickly evolve toward lobe field line reconnection at a single NENL at least in a given local time sector. It is the high-speed flow out of this NENL that sweeps away the magnetic flux ropes formed during the closed field reconnection phase. The individual flux ropes are carried toward and away from the Earth depending upon whether a given rope is Sunward or anti-Sunward, respectively, of the *X*-line that first begins to reconnect lobe flux tubes and generate high-speed Alfvenic jets.

2. BBF-Type Flux Ropes

[10] An example of a BBF-type flux rope event with a very strong core field on 27 January 1996 is shown in Figure 2a. A clear bipolar south-then-north rotation of B_z is present at 20:35:30. Coincident with the inflection point in the B_z variation are enhancements in B_x and B_y. Further-

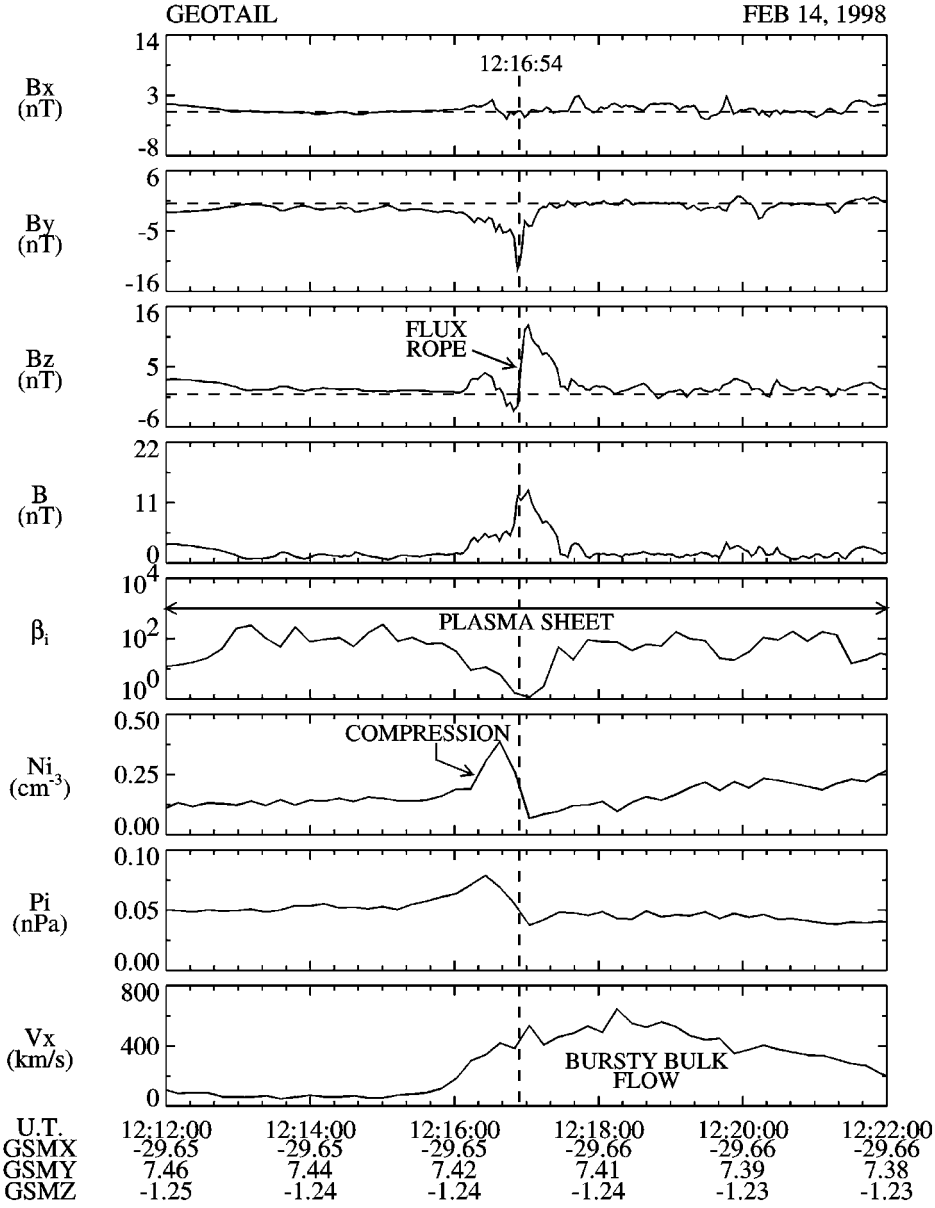

Figure 3. Geotail magnetic field and plasma measurements taken on 14 February 1998 of a BBF event containing an embedded flux rope. Note that the flux rope occurs about 1 min after the start of the bursty bulk flow event.

more, the B_x and B_y enhancements give rise to a peak in total field intensity (see bottom panel) that is ~1.9 times greater than the adjacent lobe region magnetic fields. The flux rope duration based upon the B_z signature is ~15 s.

[11] In Figure 2b the merged Geotail magnetic field and LEP plasma measurements are displayed [*Mukai et al.*, 1994]. The ratio of thermal ion pressure to magnetic pressure, β_i, in the fifth panel from the top is used to identify the various tail regions. Plasma beta less than 0.1 is generally associated with the lobe region while 0.1–0.3 correspond approximately to the plasma sheet boundary layers (PSBL) and $\beta_i > 0.3$ is considered the plasma sheet proper [e.g., see *Baumjohann et al.*, 1990; *Mukai et al.*, 1996]. As shown, this flux rope was located in the plasma sheet. Further inspection of the V_x panel at the bottom of Figure 2b indicates that it was closely associated with start of a bursty bulk flow event which reached a peak speed of ~600 km/s. The ~15 s duration of the magnetic signature and the ~374 km/s flow speed at the time of the flux rope passage imply a diameter of ~1 R_E.

[12] A second example of a BBF-type flux rope is shown in Figure 3. As shown, this 14 February 1998 event had magnetic field signatures very similar to those observed in the previous event with the peaks in B_y and B_x coincident with the $\mp B_z$ variation. The flux rope is immersed in central plasma sheet with the ion beta before and after near 100. Within the flux rope, β_i decreases to unity at the point of peak magnetic field intensity, but this appears due primarily to the increase in magnetic field intensity as opposed to any change in ion pressure. Hence, it might be inferred that the

high magnetic pressures within the flux rope must be "self-balancing". As with the previous example, the flux rope was embedded in fast plasma sheet flow with the flux rope following the onset of the BBF by about a 1 min. The duration of the BBF was ~6 min with a peak flow speed just over 600 km/s. A clear compression of the plasma sheet is apparent just ahead of the flux rope. The duration of the flux rope was 28 s and the flow speed was 384 km/s so that the implied flux rope diameter was ~1.7 R_E.

[13] To obtain a population of flux ropes for statistical analysis and modeling purposes, the Geotail magnetic field observations collected between 1 November 1998 and 30 April 1999 have been surveyed to identify flux rope events between $X \sim -10$ and -30 R_E. As discussed earlier, the signature of Earthward moving flux ropes oriented along (or opposite) the GSM Y direction is a south-then-north B_z perturbation with a strong increase in B_y near its center. For a tailward moving rope, the sense of the B_z perturbation reverses (i.e., northward-then-southward). As the orientation of a flux rope in the $X-Y$ plane moves away from the east–west direction, the core magnetic fields begin to contribute also to the B_x field component. In order not to restrict the longitudinal orientations of the flux ropes considered by this study enhancements in B_x or B_y coincident with $\pm\Delta B_z$ on times scales of a few seconds to a few minutes were identified as "flux ropes". In principle, a rotation of the tail such that the plasma sheet was located near the GSM X–Z plane would result in the core fields of flux ropes appearing largely in the B_z and B_x components in association with a $\pm\Delta B_y$ perturbation. While such large rotations are known to occur in the distant tail [*Sibeck et al.*, 1986; *Owen et al.*, 1995], they are not expected to be a significant factor in the identification of flux ropes at X >– 30 R_E.

[14] The approach taken was to closely examine intervals when Geotail was located in or near the plasma sheet in order to identify all ± or ∓ variations in the GSM B_z component on timescales of seconds to minutes. Typically, B_z in the plasma sheet is positive at these downtail distances. For our survey it was required that B_z reach negative values, but not that the perturbation be symmetric about $B_z \sim 0$. Although the fields associated with the flux ropes should not transport any net B_z flux, the interaction of the flux ropes and the fast flows in which they are embedded with the surrounding plasma sheet can produced a "pile-up" of north–south oriented magnetic flux ahead and/or behind these events [see *Nagai et al.*, 1998b; *Slavin et al.*, 1998]. This often results in asymmetric B_z perturbations in which the positive and negative flux is not balanced. The events were then further culled to eliminate those lacking coincident enhancements of the GSM B_y and/or B_x field components in order to separate "ropes" from "loops". In summary, so long as flux rope orientations do not approach either the X or Z axes so closely that the amplitude of their ± B_z perturbation go to zero then they should be included in the events selected for analysis by this study.

[15] The locations of the 35 BBF-type flux ropes identified in this manner are shown in Figure 4. The events were evenly spread over the region from GSM $X \sim -14$ to -30 R_E and GSM $Y \sim +15$ to -15 R_E. The north–south distribution, GSM $Z \sim -4$ to +6 R_E, simply corresponds to the range of values over which the plasma sheet was

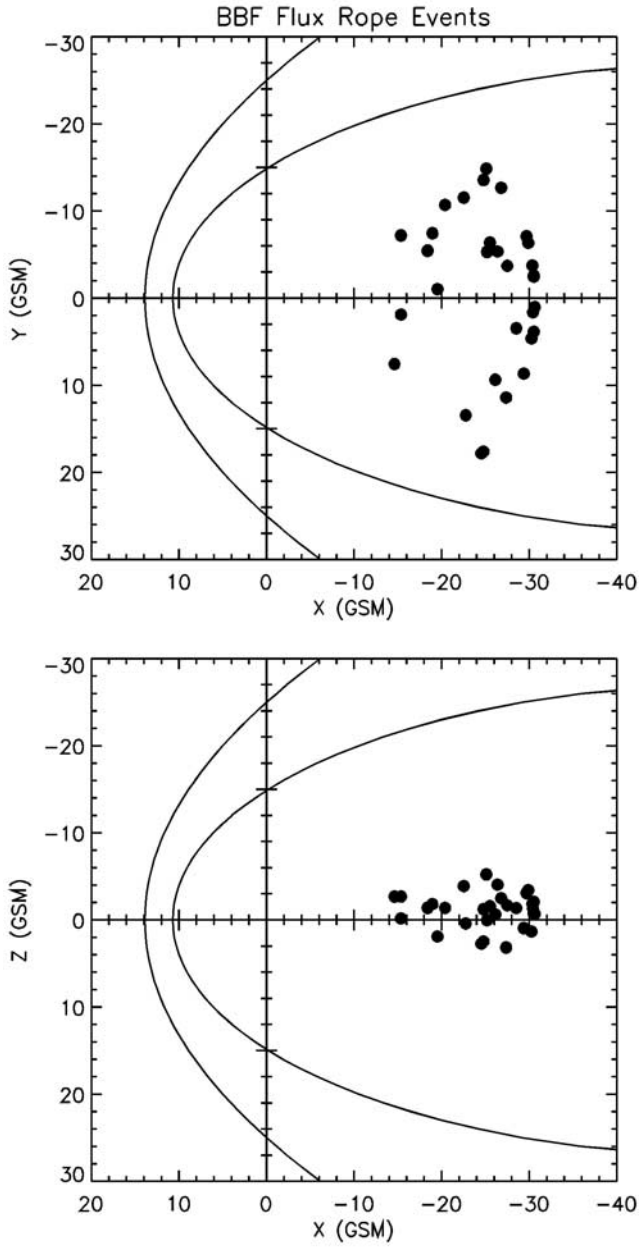

Figure 4. Spatial distribution of the 35 BBF-type flux rope events identified during the 1998–1999 Geotail nightside apogee season.

sampled by Geotail. Very similar event distributions were found in previous Geotail studies of high-speed flows [e.g., *Nagai et al.*, 1998a; *Fairfield et al.*, 1998]. Figure 5 presents a superposed epoch analysis of the magnetic field perturbations associated with these flux ropes using 1 s averaged data. The time domain is ±120 s and the midpoint of the B_z signature was taken as the zero epoch (i.e., the midpoint between the extremes in the $\pm B_z$ excursions). The midpoint of the B_z crossing is often not the zero-crossing, but it tends to be highly correlated with the peaks in B_x, B_y and B_{total}. For this reason it was chosen as a very reproducible and appropriate zero epoch for the analysis. The basic features discussed earlier are all evident. The B_z component varied from ~−2 to +9 nT. The amplitude of the ΔB_y and ΔB_x

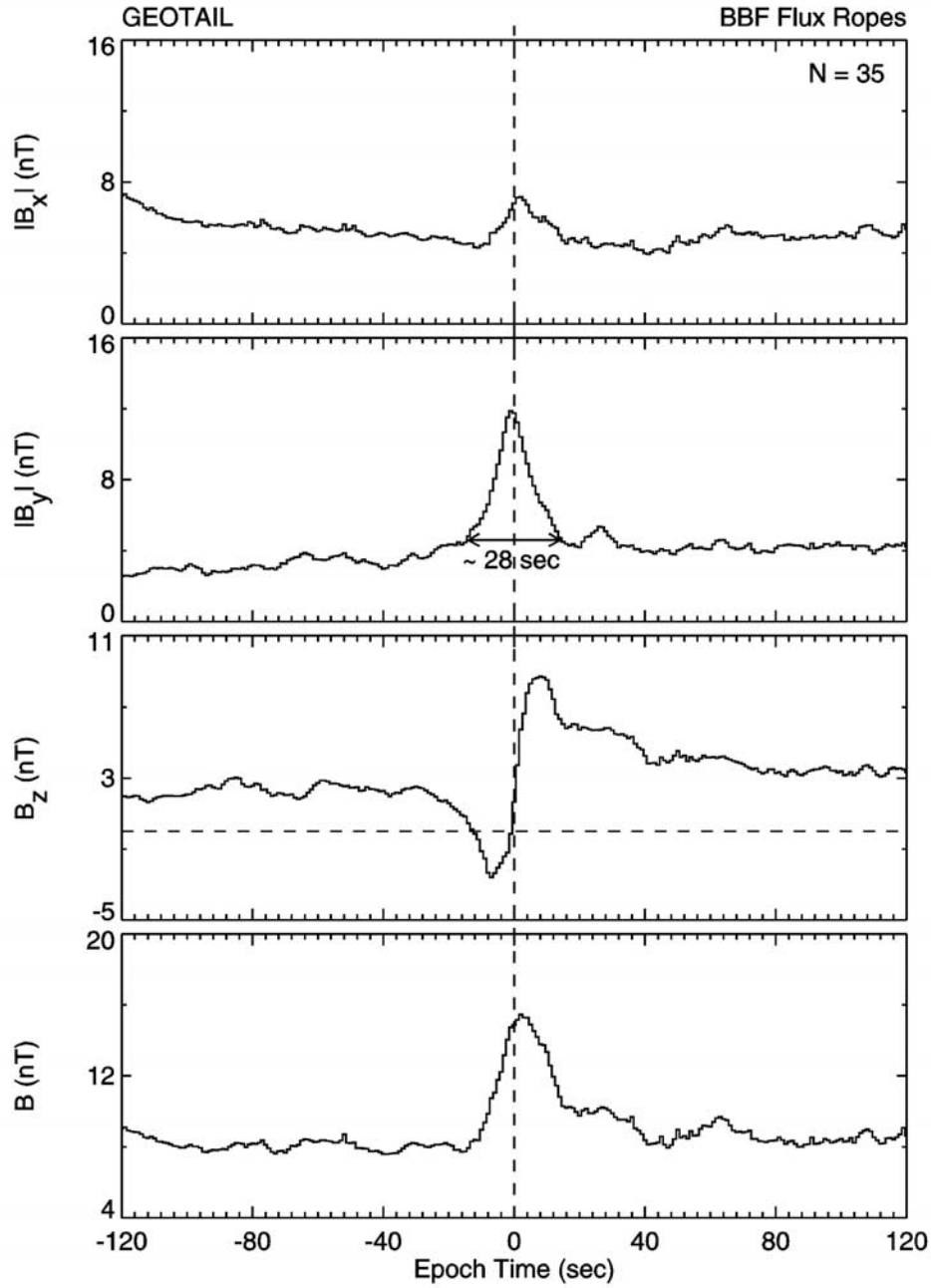

Figure 5. Superposed epoch analysis performed using 1 s averages of the Geotail magnetic field measurements for all 35 BBF flux rope events.

enhancements were ~8 and 2 nT, respectively, and the total field increased by nearly a factor of 2. Finally, the durations of the B_y and B_x enhancements were similar to that of the south-then-north B_z perturbation at ~28 s.

[16] Subsequent examination of the LEP plasma measurements revealed that all 35 of these events were, indeed, associated with Earthward bursty bulk flows. These high-speed Earthward flows typically exhibit amplitudes of a few 100 km/s to over 2000 km/s and durations from ~1 to 15 min [*Angelopolous et al.*, 1992]. In most, but not all cases identified in this study, the magnetic flux ropes were observed near the leading edge of the Earthward flow event. There were no cases of flux ropes being observed prior to the flow event. This aspect of the BBF-type flux ropes is quantified in Figure 6 where the time difference, ΔT, between the beginning of the BBF, T_{BBF}, taken to be when V_x exceeded ~100 km/s, and the midpoint of the flux rope based upon the B_z signature, T_{FR}. As shown, the most common time lag between the start of the flow burst or BBF and the passage of the flux ropes is 50 s with 25 of the 35 events exhibiting flux ropes embedded in the first 200 s of the flow event.

[17] These results are used to construct a second superposed epoch analysis, shown in Figure 7, drawing upon

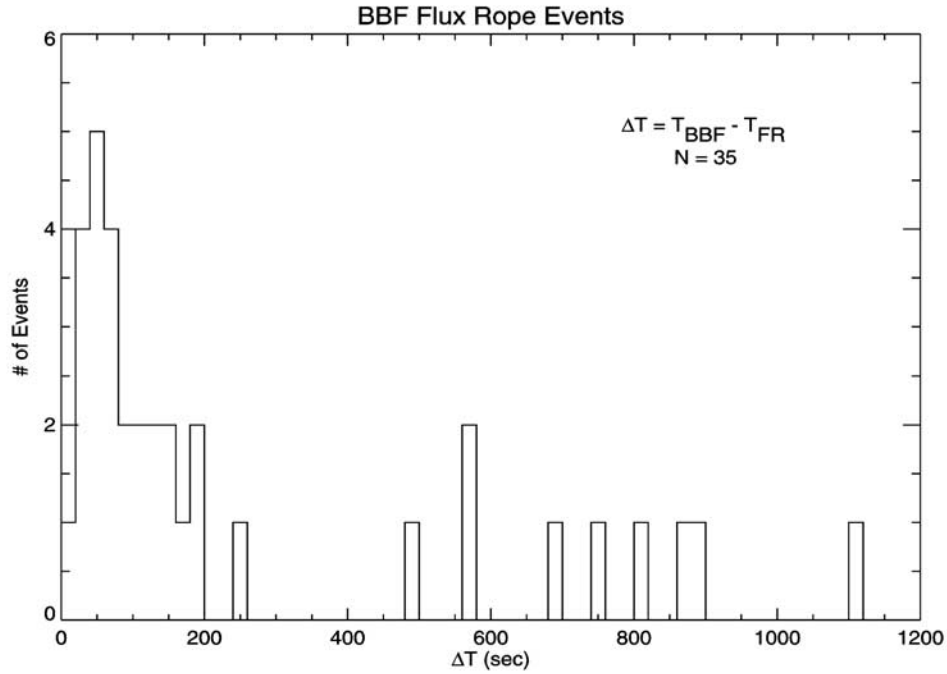

Figure 6. Histogram of the time differences between BBF onset and the passage of the center of the flux rope past Geotail for the 35 BBF flux rope events.

both the magnetic field and the plasma measurements. Again, the time domain for the analysis is ±120 s with the center of the flux rope as the zero epoch. For this purpose the 16 BBF-type flux rope events for which the time difference between the start of the Earthward flow and the center flux rope was 100 s or less were used. This selection was carried out to avoid ''smearing'' the plasma variations by including events with very different temporal phasing between the flow and the magnetic field.

[18] The flux rope magnetic signature is shown in the top two panels where B_y and B_z are plotted. The ratio of the thermal pressure of the ions to the magnetic field, β_i, is graphed in the third panel. It's high value, ~10, before and after the flux rope indicates that the spacecraft was located deep in the central plasma sheet. Within the flux rope itself, the strong magnetic fields reduced β_i to ~2–3. The BBF signature is apparent in V_x as shown in the bottom panel. The Earthward flow begins to increase quickly ~40 s prior to the flux rope and peaks at ~600 km/s about 40 s afterward. Ahead of the flux rope, where the flow speed is increasing, there is a density compression of similar duration, ~40–60 s. As with the previous displays, the standard 12 s LEP plasma bulk moments are utilized. Accordingly, it not possible to determine the plasma variations within the flux rope itself or to investigate the internal stress balance directly via equation (1).

3. Plasmoid-Type Flux Ropes

[19] As discussed earlier, an extensive literature already exists regarding plasmoids and their properties, including magnetic field topology [see *Ieda et al.*, 2001, and references therein]. However, for comparative purposes, we have also identified plasmoid-type flux ropes during the November 1998–April 1999 Geotail ''tail season''. The number of plasmoid-type flux ropes identified, 38, was similar to the number of BBF-type events discussed earlier. The locations of the 38 plasmoid flux rope events found here are shown in Figure 8. The spatial distribution of these events was very similar to that of the BBF flux ropes, i.e., $X \sim -16$ to -30 R_E, Y ~ +25 to -16 R_E, and Z ~ -6 to +6 R_E. Overall, there appears to be little difference between the plasmoid-type and BBF-type flux rope populations in the near-tail with respect to their frequency of occurrence or spatial distribution.

[20] As with the BBF-type flux ropes, all 38 of these plasmoid-type events were associated with high-speed plasma sheet flow, but, as expected, in the tailward direction. Again, the difference between the beginning of the fast tailward flow, T_{TF}, taken to be when V_x was less than ~-100 km/s, and the midpoint of the flux rope, T_{FR}, was examined with similar results to those found of the BBF flux ropes. The distribution of delay times (not shown) was somewhat narrower than was the case for the BBF flux ropes. Indeed, all of the plasmoid-type events accompanied the onset of fast tailward flow within ~200 s and 31 with $\Delta T < 100$ s. The most common time lag between the start of the flow burst and the passage of the flux ropes was ~40 s which is very close to the result for BBF-type flux ropes.

[21] A superposed epoch analysis of the 31 plasmoid-type flux rope events observed within 100 s of the onset of fast tailward flow is shown in Figure 9. Again, the time domain is ±120 s with the midpoint of the flux rope taken as the zero epoch. The basic features found earlier for the BBF-type flux ropes are, again, evident. The B_z variation was nearly symmetric about zero and varied from ~+3 to -3 nT. This may indicate that the tailward moving flux ropes do not usual experience as much ''pile-up'' due to the subsequent flow out of the *X*-line as do their Earthward moving BBF-type counterparts. The amplitude of the ΔB_y enhancement was ~4 nT or a little less than was seen for the BBF-

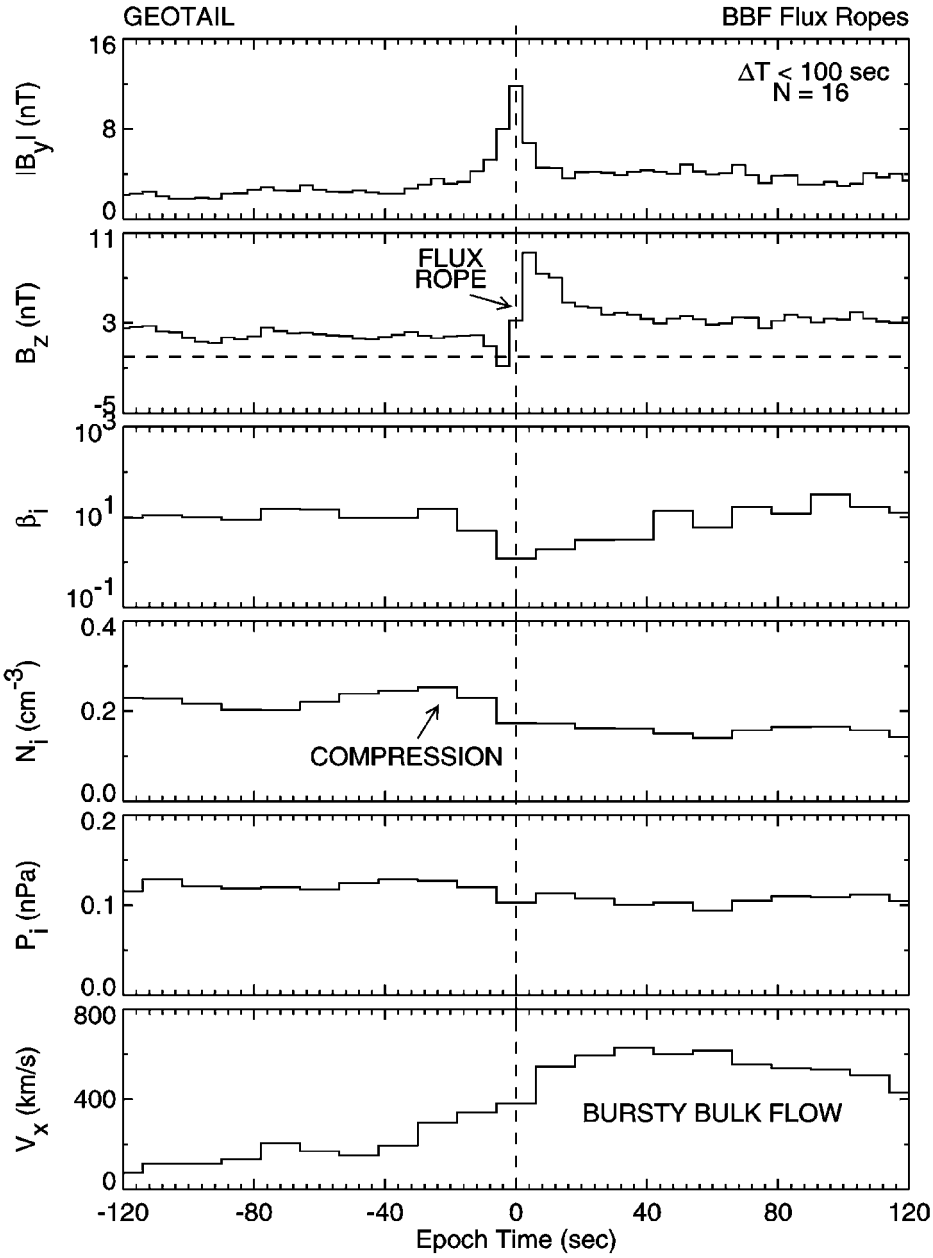

Figure 7. Superposed epoch analysis using both magnetic field and plasma measurements for the 16 BBF flux rope events for which the flux rope passage occurred within 100 s of the BBF onset.

type ropes. The duration of the magnetic intensity increase was similar to that of the south–north B_z perturbation at ~32 s, or nearly equal to the duration of the BBF flux ropes. The superposed epoch analysis also shows that the ratio of the thermal pressure of the ions to the magnetic field, β_i (see the third panel) is uniformly high at a value of near 10. This is very similar to that observed for the BBF-type flux ropes, but no changes in the plasma parameters were detected within the flux rope itself. Perhaps, this is because the plasmoid-type flux rope core fields are not so intense as with the BBF-type ropes. Finally, the superposed plasma velocity is shown in the bottom panel. The tailward flow begins to increase quickly ~40 s prior to the flux rope and peaks at ~−500 km/s. Ahead of the plasmoid-type flux rope, where the flow speed initially decreases there is a modest density compression.

4. Flux Rope Modeling

[22] In order to model the flux ropes presented here we will assume them to be approximately force-free structures [e.g., *Goldstein*, 1983; *Marubashi*, 1986] wherein the current density (**J**) and the magnetic field (**B**) are parallel or antiparallel;

$$\mathbf{J} = \alpha \mathbf{B} \tag{2}$$

Their geometry is that of a nested set of helical magnetic field lines confined to a flux tube, as shown earlier in Figure 1.

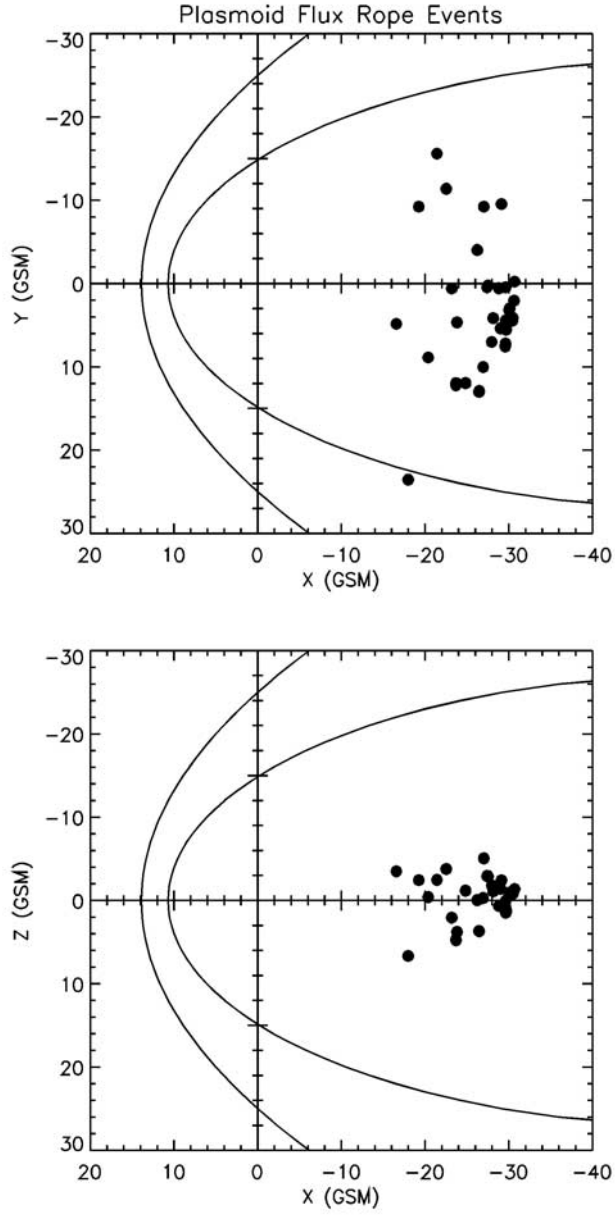

Figure 8. Spatial distribution of the 38 plasmoid-type flux rope events identified during the 1998–1999 Geotail nightside apogee season.

The structure is assumed to be cylindrically symmetric with the pitch angle of the helical field lines increasing with growing distance from the axis of the rope. Hence, the field at the center of the rope is aligned with its central axis, but perpendicular to this axis at the outer boundary of rope. An analytical approximation for this field configuration is the static, constant-α, force-free, cylindrically symmetric configuration given by the *Lundquist* [1950] solution to

$$\nabla^2 \mathbf{B} = -\alpha^2 \mathbf{B} \tag{3}$$

that results from equation (2) and the use of Maxwell's equations [e.g., *Burlaga*, 1988]. The Lundquist (Bessel function) solution is:

$$B_z(r) = B_O J_0(\alpha r),\ B_\theta(r) = B_O H J_1(\alpha r),\ \text{and } B_r = 0 \tag{4}$$

Where B_o is the peak field intensity along the axis of the flux rope, H = ±1 is the rope's handedness and α is considered positive.

[23] We have fit the *Lundquist* [1950] solution of equation (3) to **B** (in GSM coordinates) across the flux rope events discussed in the previous sections using the method of *Lepping et al.* [1990]. This approach was originally applied to interplanetary magnetic clouds with flux rope magnetic topologies. Initially, only the field's direction is considered in the form of unit normalized magnetic field data. A variance analysis is applied to these data in order to establish an approximate rope coordinate system. The flux rope's axis is usually close to the intermediate variance direction from this analysis. We then perform a least squares fitting between the normalized, observed magnetic field after transformation into this initial coordinate system and the expressions in equation (4). The least squares fitting usually results in a slight modification of the initial estimate of the axial direction. Once the orientation of the flux rope relative to the spacecraft trajectory has been determined, the radius of the flux rope is inferred using the measured V_x plasma flow speed.

[24] A "reduced chi" to the fit, $\chi_R/(3N - n)$, is used to measure the quality of the fit, where N is the number of points considered in the analysis interval (i.e., essentially the rope duration), and n = 5 is the number of parameters used in the fit. The chi-quantity parameter is dimensionless since the magnetic field was unit normalized up to this point. A $\sqrt{\chi_R}^2 = 0.04$ or less is required before a fit is regarded as "acceptable" [see *Lepping et al.*, 1990]. The quality of fit is judged, secondarily, on the symmetry of the fitted field intensity profile. We define an asymmetry factor, $ASF = |(1 - 2t_O/(N-1))|$, where t_O is the center time of the rope in terms of the number of sample points, N. An ASF of 0 is ideal, and anything over 0.5 is not acceptable. Finally, a simple linear scaling of the model field's magnitude to the observed field's magnitude is done taking into consideration the model estimate of the closest approach distance, Y_o, of the spacecraft to the rope's axis.

[25] Accordingly, the full set of flux rope-fitted parameters are: B_O, the axial field intensity; H, the handedness of the field twist (±1 for right/left handedness); R_O, the radius of the flux rope; Φ_A, Θ_A, the longitude and latitude of the rope's axis, respectively; t_O, the rope center time; and Y_O/R_O, the "impact parameter". Note that we ideally choose the boundaries of the flux rope such that the magnetic field becomes purely azimuthal at those points (i.e., where αr = 2.4). However, in practice this is not always possible, and the exact end-points are not always evident in the data. For this reason trial-fits are generally necessary with the best choice being based on the reduced-chi and asymmetry "quality" factors as discussed above.

[26] Model fits to the 27 January 1996 BBF-type flux rope discussed earlier are presented in Figure 10a. This is an example of an excellent fit between the Lepping-Burlaga flux rope model and actual Geotail observations. Dashed and solid vertical lines mark the selected beginning and end of the fitting interval. The best fit constant-α model is shown with solid curves. The reduced chi and ASF asymmetry parameters were very small at 0.01 and 0.02, respectively, i.e., the fit is excellent with the peak field strength being located very close to the middle of the rope. The

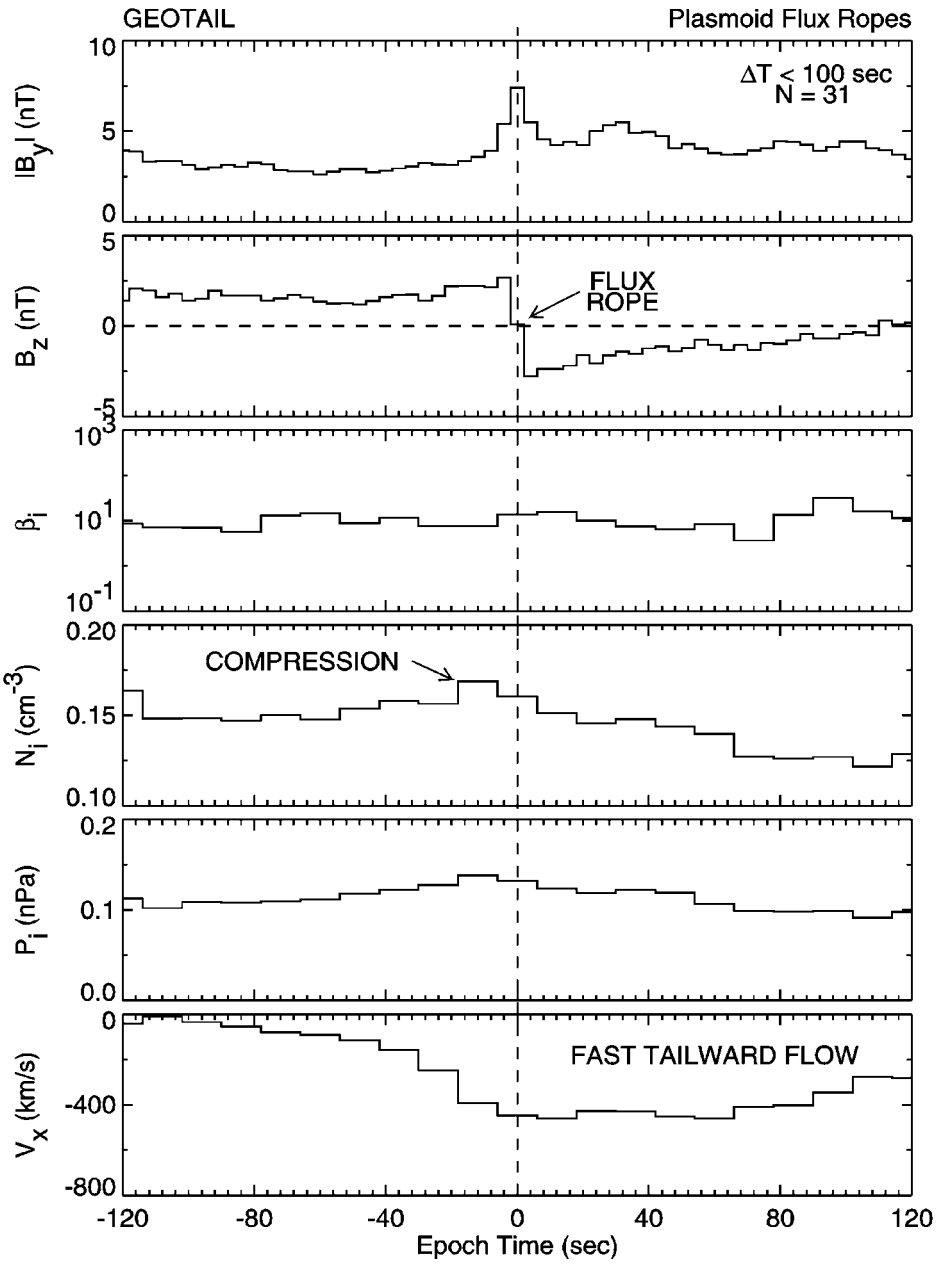

Figure 9. Superposed epoch analysis using both magnetic field and plasma measurements for the 31 plasmoid flux rope events for which the flux rope passage occurred within 100 s of the plasmoid flow onset.

radius of the flux rope inferred from the model is 0.6 R_E (i.e., the diameter is 1.2 R_E) and the maximum magnetic field intensity along the central axis of the rope, B_o = 26.3 nT. This compares with the flux rope diameter estimated earlier at 0.9 R_E on the basis of the observed V_x and duration of the flux rope encounter. The spacecraft closest approach distance, Y_o, was very near the central axis with Y_o/R_o = 0.08. Consistent with this small impact parameter, the observed and modeled peak fields are very similar in magnitude. The orientation of the rope was very near the GSM X–Y plane, latitude angle $\Theta = 4°$, and a longitude angle of $\Phi = 291°$ which is close to the dawnward direction.

[27] Figure 10b presents the modeling results for the 14 February 1998 BBF-type flux rope, also discussed earlier. This is an example of a marginal, but acceptable fit according to our criteria. In particular, it is very apparent that the B_y field increase, while nicely centered in the $\pm B_z$ variation, is much narrower than predicted by the model. Furthermore, there are higher order perturbations in all three components of the field and the total intensity. Still, the reduced-chi parameter was an acceptable 0.02, cf. our maximum acceptable value of 0.04, and the asymmetry parameter, ASF, was a fairly good at 0.2. The radius of the flux rope inferred from the model is 1.0 R_E (i.e., the diameter is 2.0 R_E) and the maximum magnetic field intensity along the central axis of the rope is B_o = 12.0 nT. This compares reasonably well with the flux rope diameter estimated earlier at 1.7 R_E on the basis of the observed V_x

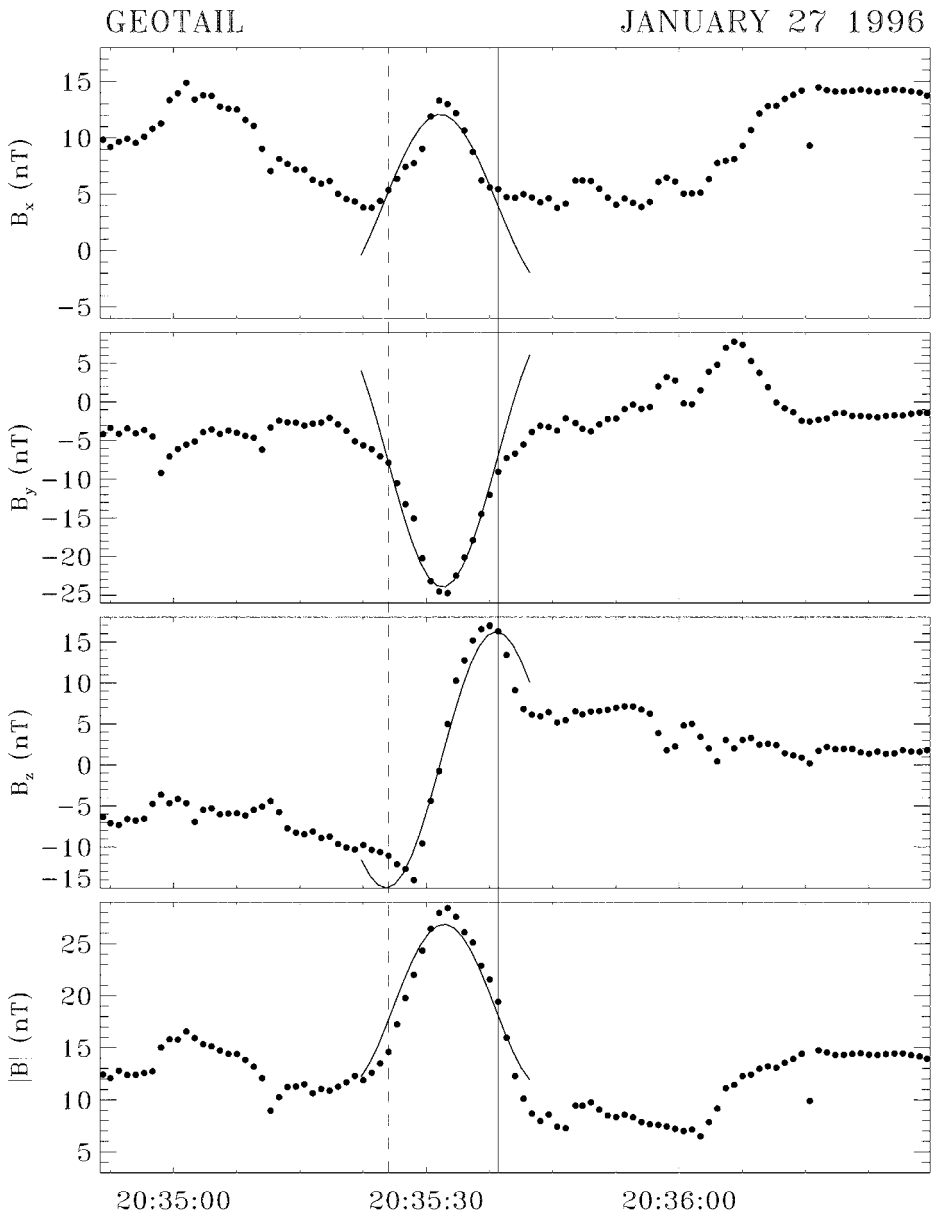

Figure 10a. Comparison of a force-free flux rope model (solid line) against actual magnetic field measurements for the 27 January 1996 flux rope event displayed earlier.

and duration of the flux rope encounter. The spacecraft closest approach distance was moderately close to the central axis with $Y_o/R_o = 0.19$. The peak observed magnetic field is somewhat higher than the model probably because of its narrowness relative to the constant-α model. This rope had one of the largest latitude angles measured in this study with $\Theta = 43°$ while the longitudinal orientation as largely dawnward at $\Phi = 282°$.

[28] When these fitting procedures were applied to all of the flux ropes identified in this study, acceptable force-free flux ropes fits were found for 21 out of the 35 BBF-type events and 23 out of the 38 plasmoid-type events for an overall success rate of ~60%. The fitted model parameters for all of the BBF and plasmoid-type flux ropes are shown in Figures 11a and 11b. The top row in each figure presents the properties of the BBF-type flux ropes while the bottom row addresses the plasmoid-type events. In Figure 11a the mean core field intensity and diameter for the BBF and plasmoid-type ropes are 20.3 nT and 1.4 R_E and 13.5 nT and 4.4 R_E, respectively. Interestingly, both types of flux rope have a peak in the distribution of rope radius under 1.0 R_E, but the plasmoid-type event distribution has a "tail" with radii going up to 6 R_E. The distribution of the ratio of Geotail closest approach distance to flux rope radius is relatively flat, albeit with a maximum at small values in both cases, with means of 0.4. Finally, the V_x bulk plasma speeds measured within the two populations by Geotail are histogrammed in the panels to the far right. This measured speed is used by the magnetic field modeling procedure to infer the physical dimensions of the flux ropes. The mean Earthward and tailward flux rope speeds are nearly the same at +431 km/s and −451 km/s, respectively.

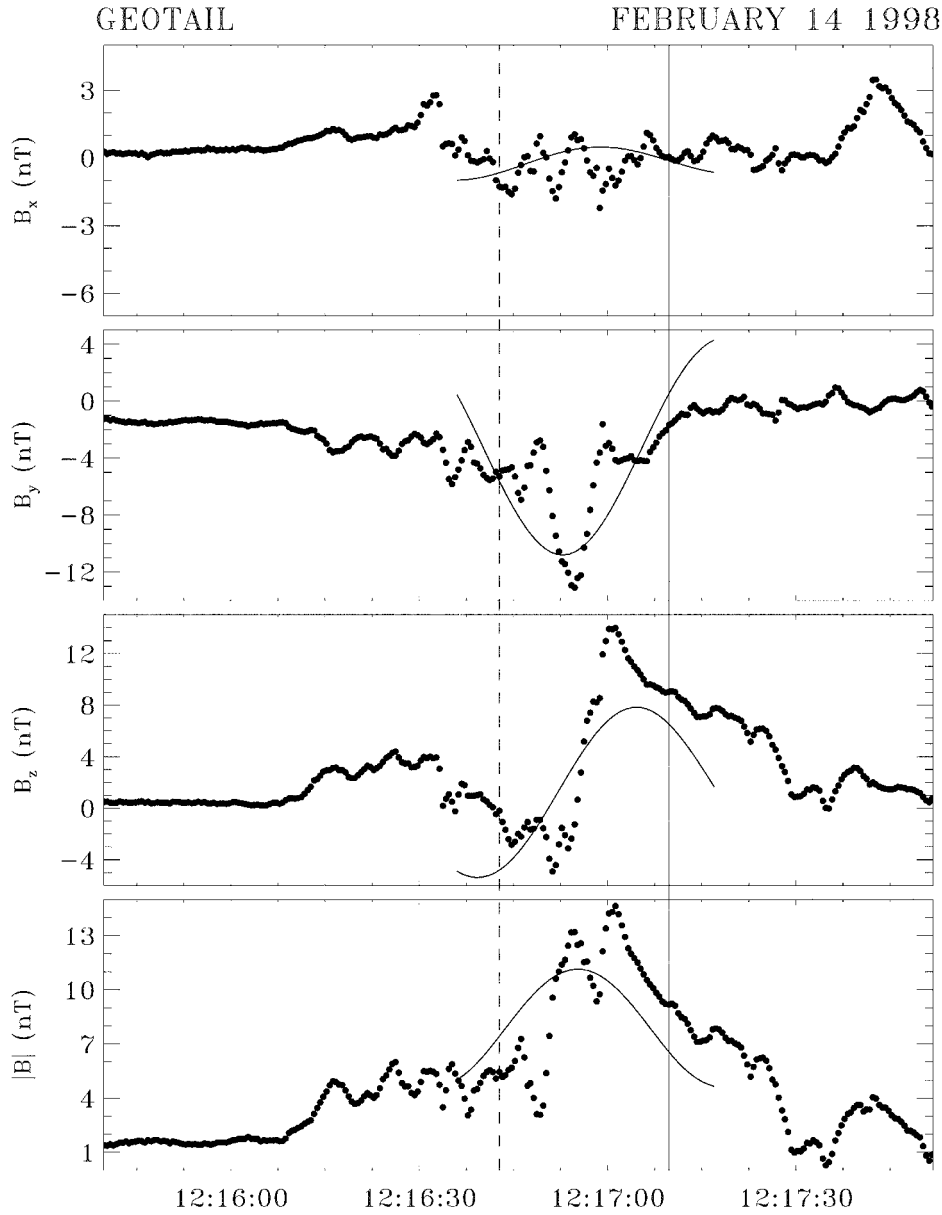

Figure 10b. Comparison of a force-free flux rope model (solid line) against actual magnetic field measurements for the 14 February 1998 flux rope event displayed earlier.

[29] The orientations of the two flux rope populations are addressed in the leftmost panels of Figure 11b. The latitude angle, Θ, of the flux rope (i.e., along the direction of the core magnetic field) is measured such that -90 and $90°$ are directed toward the south and north, respectively, while $0°$ corresponds to the GSM equatorial plane. The BBF and plasmoid-type flux ropes directional distributions are centered in the GSM X–Y plane with mean latitude angles of only $10°$ and $1°$, respectively. However, a wide range of longitudinal direction was determined. Some maxima are observed near the dawn, $\Phi = 90°$, and dusk, $\Phi = 270°$, directions, but the distributions appear very broad. (Mean angles for Φ greater or less than $180°$ are shown.) Another output of constant-α flux rope model is the total amount of magnetic flux they contain [e.g., *Lepping et al.*, 1996]. In this case, the large radii of some of the plasmoid-type events results in a mean magnetic flux content of 9.1×10^{14} Mx as opposed to 1.1×10^{14} Mx for the BBF-type flux ropes. For comparison, the magnetic flux contained in each tail lobe is $\sim 5 \times 10^{16}$ Mx [e.g., *Slavin et al.*, 1985]. Hence, the magnetic flux carried by the plasmoid and BBF-type flux ropes is small at only $\sim$2% and 0.2%, respectively, the flux content of each lobe.

[30] Consistent with previous studies of plasmoids [*Hughes and Sibeck*, 1987; *Moldwin and Hughes*, 1991], the observed polarity of the B_y in the central core of the flux ropes agreed with half hour averages of IMF B_y in 14 of 15 and 8 of 13 events for the BBF- and plasmoid-type flux ropes for which there were upstream IMF data. In the rightmost panels of Figure 11b this relationship is further examined by graphing flux rope core field, B_o against IMF B_y. (N.B., IMF B_y was averaged over a 30 min interval prior

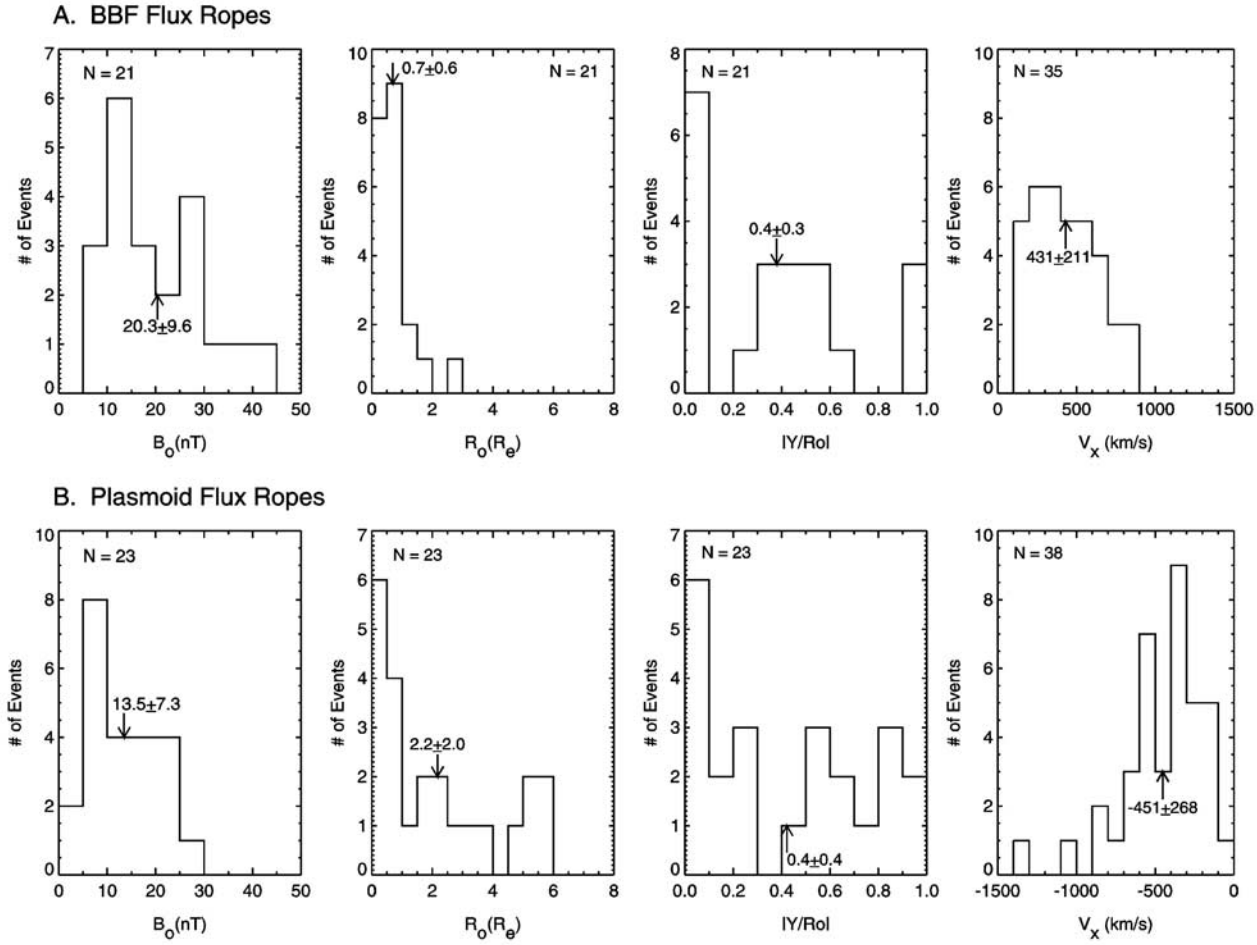

Figure 11a. Flux rope modeling results for BBF and plasmoid flux rope event size and spacecraft trajectory impact parameter, $|Y/R_o|$. A distribution of the measured flux rope velocities, measured by the Geotail plasma analyzer and used as an input to the analytical modeling, is also provided.

to the arrival of the flux rope at Geotail after a correction was made for the propagation time from the solar wind monitor to Geotail.) Separate linear regressions produced fits passing near the origin with slopes of order unity, i.e., 2.6 and 1.6, respectively. The correlation coefficients were 0.7 and 0.4 for the BBF and plasmoid-type flux ropes. The reason for the poorer correlation in the latter case is unclear, but it should be noted that the range of IMF B_y values was not so wide as for the plasmoid-type flux ropes and more closely clustered about $B_y \sim 0$. Overall, the basic scenario for flux rope formation in the tail described earlier appears well supported by these results.

5. Discussion

[31] The most important result of this investigation is that small, $\sim 2-5\ R_E$ diameter magnetic flux ropes are relatively common in the near-tail plasma sheet. Geotail took approximately 1400 hours of measurements between $Y = \pm 18\ R_E$ and $X = -14$ to $-30\ R_E$ during the November 1998 and April 1999 tail season. If 25% of these observations corresponded to the central plasma sheet, then the frequency of occurrence for these flux ropes is 0.2 hr^{-1} or 1 flux rope event per 5 hours of central plasma sheet observing time. Although a detailed examination of the relationship between these flux rope events and substorm activity is beyond the scope of the present study, it should be noted that this rate is comparable to typical substorm occurrence rates in the near-tail [e.g., *Angelopoulos et al.*, 1996].

[32] Flux rope properties have been determined using the well tested Lepping-Burlaga constant-α, force-free flux rope model [*Lepping et al.*, 1990]. The use of such a model is very desirable because it takes the observed magnetic field variations and infers the large-scale orientation and properties of the flux rope. In the absence of such modeling, simple statistical analyses of the measured properties would be heavily influenced by the trajectories of the spacecraft relative to the central axis of the flux rope. For example, equating the mean peak magnetic field measured during the various Geotail flux rope encounters with the actual mean core magnetic field intensity could easily result in underestimates of up to a factor of 2. The constant-α modeling yielded mean flux rope diameters and core field intensities of 1.4 R_E and 20 nT and 4.4 R_E and 14 nT for the BBF- and plasmoid-type flux ropes, respectively.

[33] The inclinations of the flux ropes were small relative to the GSM $X-Y$ plane, but a wide range of longitudinal

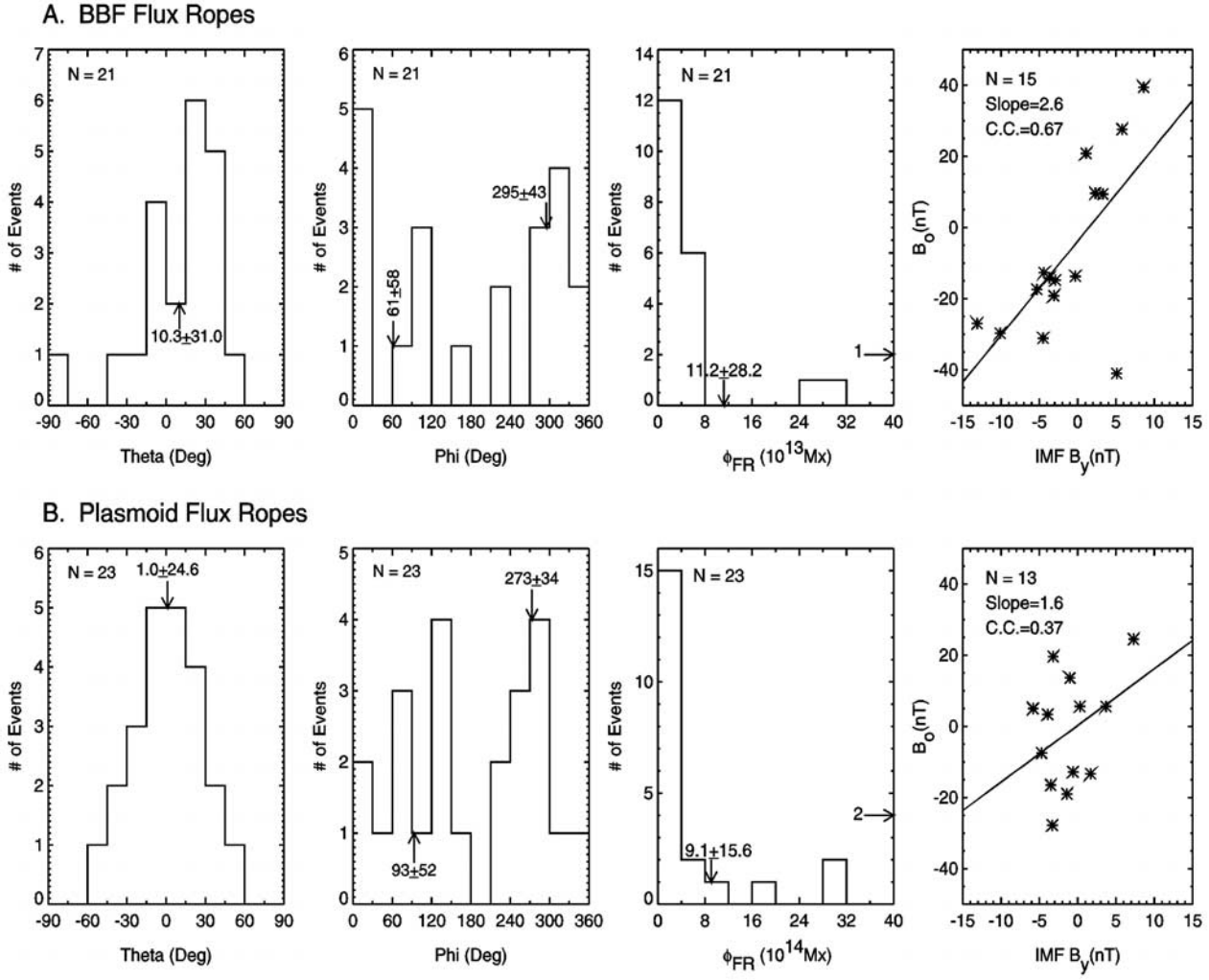

Figure 11b. Flux rope modeling results for BBF and plasmoid flux rope event orientation, core field magnitude and correlation between core field direction and strength versus IMF B_y.

orientations were determined within that plane. The great variability in the azimuthal orientation of the flux ropes appears to support a prediction by *Hughes and Sibeck* [1987]. They speculated that during the plasmoid formation process either the dawn or dusk ''end'' of the flux rope might remain strongly connected to the Earth longer than the other end. The drag exerted on the end still connected to the Earth would then skew the flux rope azimuthal orientation away from the dawn–dusk direction when the flux rope is swept tailward. For BBF-type flux ropes similar arguments can be made involving magnetic connection to the more distant tail or IMF. Such scenarios could account for the wide distribution of azimuthal distributions determined by our study. However, temporal variations in the flow coming out of the reconnection *X*-line(s), local time variations in the reconnection rate and/or variations in the plasmas and magnetic fields with which the high-speed flows and flux ropes collide could also cause the observed broad distribution of flux rope longitudinal orientations. Although difficult or impossible to infer from single spacecraft measurements, a full understanding of the orientation of these flux ropes requires a knowledge of at least the 2-D plasma sheet flow pattern so that the effects of ''shear'' and ''rotation'' can be evaluated [see *Sergeev et al.*, 1996].

[34] In addition, the relative success of the Lepping-Burlaga model in representing the magnetic field variations both in the BBF and plasmoid-type flux ropes suggests that $\mathbf{J} \times \mathbf{B}$ forces may be small within these structures. The force-free nature of the plasmoid-type flux ropes has long been presumed due to their very strong core fields, in extreme cases a factor of 2 greater than the adjacent lobe magnetic fields. Such large magnetic fields must be largely ''self-balancing'' or an equilibrium with the surrounding tail would not be possible [e.g., see *Slavin et al.*, 1995]. In addition, the good quality of the fits to the flux rope model strongly suggests that these structures are also fairly cylindrical in shape. Strong deviations from cylindrical geometry might have been expected either as a result of the formation process or due to dynamical stresses exerted as these structures are swept Earthward/tailward and interact with the surrounding plasma sheet.

[35] The small diameters of the flux ropes and their high speeds results in the spacecraft residing within these structures for only a few seconds to several tens of seconds. As a

result, we typically obtain only a few 12 s plasma parameter determinations within each flux rope. Accordingly, it is not surprising that the superposed epoch analyses in Figures 7 and 9 show little variation in the bulk plasma parameters associated with the flux ropes themselves and it is not possible to perform any detailed examination of the flux rope stress balance condition described in equation (1). The most intense plasma variation for both types of flux rope events is the compression in ''front'' of the events that is almost certainly due to the fast flows ''snow plowing'' into the undisturbed ''upstream'' plasma sheet. For the BBF-type flux ropes, which have more intense core fields than the plasmoid-type, there is a decrease in plasma beta relative to the surrounding plasma sheet. However, this result is clearly associated with the very strong magnetic fields in the core of the flux rope as opposed to any plasma variation.

[36] The determination that Earthward moving flux ropes are fairly common may also offer an explanation for the so-called ''south-then-north'' traveling compression regions (SN TCRs). The more extensively studied ''north-then-south'' or NS TCRs are local compressions of the lobe magnetic field caused by the rapid tailward motion of plasmoid-type flux ropes [*Slavin et al.*, 1984, 1993]. The tailward motion of the NS TCRs was inferred both from their characteristic north-then-south B_z signature and substorm association. Specifically, the time delay between substorm onset and the observation of a TCR, or the underlying plasmoid-type flux rope, increases linearly with the downtail distance of the spacecraft [*Slavin et al.*, 1993; *Nagai et al.*, 1994]. However, *Moldwin and Hughes* [1994] investigated TCRs in the IMP 8 tail observations and found that about a third of the compressions had the south-then-north signature. Such SN TCRs had been noted earlier [*Slavin et al.*, 1993], but they had been attributed to external compression of the tail lobes by short duration enhancements of solar wind pressure. In fact, *Moldwin et al.* [2001] examined 21 SN TCRs and found that 17 were associated with short duration upstream solar wind pressure increases. However, they suggested that the remaining 4 events might be due to the Earthward moving ''plasmoids''. Indeed, the BBF-type flux ropes found in this study closely resemble the Earthward moving plasmoids hypothesized by Moldwin and Hughes and they may be responsible for the generation of the SN TCR population that is not due to external solar wind pressure increases.

[37] Still, the importance of our observations of BBF- and plasmoid-type flux ropes is not due to the energy or electrical current carried by these structures or their role in causing lobe field compressions. It can be readily demonstrated, for example, that the magnetic energy carried in these high-speed flows is quite small relative to the plasma thermal and kinetic energy [see *Slavin et al.*, 1993; *Angelopoulos et al.*, 1996; *Ieda et al.*, 1998]. In addition, the magnetic flux channeled by the ropes represents a small fraction of the total B_y magnetic flux in the plasma sheet generated by the east–west stress exerted by the IMF. Rather, the significance of the observation of these flux ropes is that their formation can most easily be understood in terms of multiple reconnection *X*-lines (MRX) in the near-tail. MRX reconnection has been extensively investigated following the observation of magnetic flux ropes at the dayside magnetopause (see the review by *Lee* [1995]). As illustrated in Figure 12a, the simultaneous reconnection of tail field lines at N + 1 *X*-lines leads to the generation of N flux ropes (plus the disconnection of the closed magnetic flux tailward of this region). The sense of the flux ropes' helicity is largely determined by the direction of the IMF B_y as predicted, for example, by *Hughes and Sibeck* [1987]. The idea that a large segment of the strongly thinned cross-tail current layer might become unstable to reconnection is not new. Such a concept is central to tearing mode models of reconnection going back to *Schindler* [1974] as well as more recent particle simulations of collisionless reconnection [*Hesse et al.*, 1999] and theories of turbulent reconnection [*Goldstein et al.*, 1986].

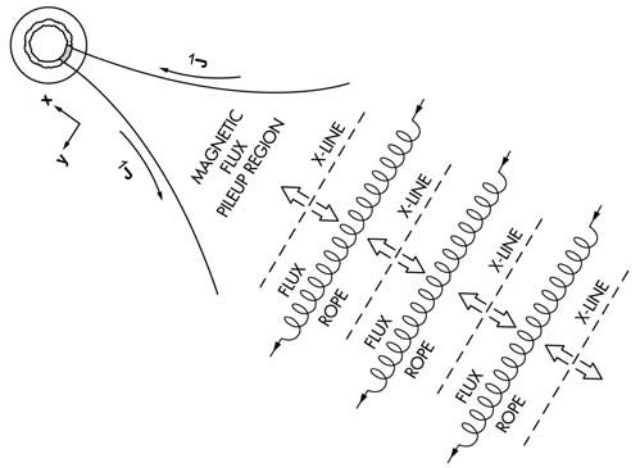

Figure 12a. Schematic depiction of the formation of earthward and tailward moving flux ropes as a result of multiple, simultaneous reconnection neutral lines in the *X*–*Y* plane.

[38] The orthogonal view of BBF- and plasmoid-type flux rope formation in the GSM *X*–*Z* plane is presented in Figure 12b. As discussed earlier, the reconnection at these multiple *X*-lines involves only closed plasma sheet flux tubes. Furthermore, the Alfven speed is quite low in the central plasma sheet so that the reconnection will proceed slowly and the outflow from the *X*-lines will be only ~10–100 km/s. However, as first argued by *Schindler* [1974], one of the *X*-lines will inevitably outpace the others and begin to reconnect first the outer plasma sheet, then the PSBL and, finally, lobe flux tubes where $V_A \sim 1000$ km/s or higher [see *Hesse et al.*, 1996]. At that point, everything Earthward of the first *X*-line to reconnect lobe flux tubes will be carried toward the Earth, and all material tailward will be rapidly swept down the tail. Hence, the formation of flux ropes by MRX reconnection is in a sense only a preliminary event to the open flux reconnection at a single neutral line in the NENL model of substorms [*Baker et al.*, 1996].

[39] Finally, these observations also raise some interesting questions regarding the ''fate'' of flux ropes in the plasma sheet. The BBF-type flux ropes carried toward the Earth and pushed up against the geomagnetic field will probably dissipate very quickly, perhaps within minutes after they are observed. The reason is that the orientation of their magnetic fields is favorable for reconnection with the geomagnetic field. In fact, the lack of symmetry between their

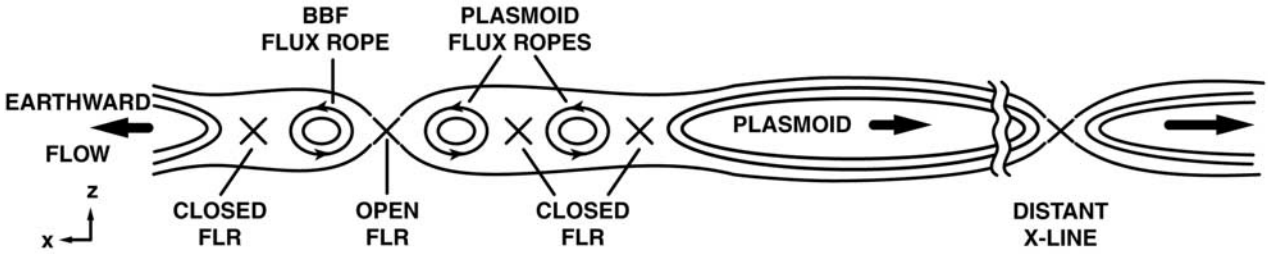

Figure 12b. Schematic depiction of the formation of earthward and tailward moving flux ropes as a result of multiple, simultaneous reconnection neutral lines in the $X-Z$ plane.

southward and northward B_z perturbations may be due in part to such "re-reconnection" having already commenced by the time their measure is taken at Geotail. Such reconnection will act to reduce the amount of southward magnetic flux along the Earthward side of the flux rope. However, of more interest is the evolution of the tailward moving plasmoid-type flux ropes. In particular, the relationship between these small flux ropes in the near-tail and the larger flux ropes observed much farther down the tail is still not clear. As illustrated in Figure 12b, in addition to the small plasmoids formed closer to the Earth, the closed field line region between the furthest of the MRX reconnection sites and the distant neutral line (DNL) should give rise to a much larger "plasmoid" containing loosely wound helical field lines. Is this the source of the large, $\sim$10 to 20 R_E long plasmoids seen by ISEE 3 and Geotail in the distant tail? Or are they due to the growth of the small flux ropes formed in the near-tail? Alternatively, do the small flux ropes collide and merge to form larger plasmoids as they move down the tail? While this question remains to be answered, it is interesting to note that some combination of these generation models may be the solution to another question regarding plasmoids; why do most plasmoids occur in groups of two or more moving down the tail in close association [*Slavin et al.*, 1993; *Shirai et al.*, 2001]? MRX reconnection in the near-tail would appear to lead naturally to tailward ejection of multiple plasmoid-type flux ropes for each substorm, just as multiple flux transfer events are common at the dayside magnetopause during intervals of southward IMF.

6. Summary

[40] Our examination of Geotail measurements has revealed that flux ropes frequently form in the near-Earth plasma sheet. A total of 73 magnetic flux ropes were identified in the Geotail magnetic field measurements between November 1998 and April 1999 for an estimated frequency of occurrence of $\sim$1 per 5 hours of central plasma sheet observations. All were embedded within Earthward or tailward high-speed plasma sheet flows. The magnetic field perturbations associated with both the BBF- and plasmoid-type flux ropes were usually observed to be simultaneous with or closely follow the onset of high-speed plasma sheet flows. Application of the Lepping-Burlaga constant-α flux rope model (i.e., $\mathbf{J} = \alpha\mathbf{B}$) to these events showed that approximately 60% of both classes of flux ropes could be reasonably well described as cylindrical, force-free flux ropes. The modeling results yielded mean flux rope diameters and core field intensities of 1.4 R_E and 20 nT and 4.4 R_E and 14 nT for the BBF and plasmoid-type events, respectively. The frequent presence of these flux ropes in the plasma sheet is interpreted as strong evidence for multiple reconnection X-lines in the near-tail. Accordingly, our observational results suggest that reconnection in the near-tail may closely resemble that at the dayside magnetopause where such events are thought to be responsible for the generation of flux transfer events.

[41] **Acknowledgments.** The expert assistance of C. Liebrecht, A. Szabo, and T. Narock with visualization and display of the Geotail measurements is gratefully acknowledged. In addition, discussions with M. Kuznetsova, M. Goldstein, D. Sibeck and V. Sergeev also contributed significantly to this research project. Finally, the authors wish to express their appreciation to all of those who have contributed to the success of the Geotail mission.

[42] Lou-Chuang and Chin S. Lin thank R. Nakamura and Jeff Hughes for their assistance in evaluating this paper.

References

Angelopolous, V., W. Baumjohann, C. F. Kennel, F. V. Coroniti, M. G. Kivelson, R. Pellat, R. J. Walker, H. Luhr, and G. Paschmann, Bursty bulk flows in the inner central plasma sheet, *J. Geophys. Res.*, *97*, 4027, 1992.

Angelopoulos, V., W. Baumjohann, C. F. Kennel, F. V. Coroniti, M. G. Kivelson, R. Pellat, R. J. Walker, H. Luhr, and G. Paschmann, Multi-Point analysis of a bursty bulk flow event on April 11, 1985, *J. Geophys. Res.*, *101*, 4967, 1996.

Baker, D. N., R. C. Anderson, R. D. Zwickl, and J. A. Slavin, Average plasma and magnetic field variations in the distant magnetotail associated with near-Earth substorm effects, *J. Geophys. Res.*, *92*, 71, 1987.

Baker, D. N., T. I. Pulkkinen, V. Angelopoulos, W. Baumjohann, and R. L. McPherron, Neutral line model of substorms: Past results and present view, *J. Geophys. Res.*, *101*, 975, 1996.

Baumjohann, W., G. Paschmann, and H. Luhr, Characteristics of high speed ion flows in the plasma sheet, *J. Geophys. Res.*, *95*, 3801, 1990.

Birn, J., M. Hesse, and K. Schindler, Filamentary structure of a three-dimensional plasmoid, *J. Geophys. Res.*, *94*, 241, 1989.

Burlaga, L. F., Magnetic clouds: Constant alpha force-free configuration, *J. Geophys. Res.*, *93*, 7217, 1988.

Cowley, S. W. H., Magnetospheric asymmetries associated with the Y component of the IMF, *Planet. Space Sci.*, *29*, 79, 1981.

Dungey, J. W., Interplanetary magnetic field and the auroral zones, *Phys. Rev. Lett.*, *6*, 47, 1961.

Elphic, R. C., C. A. Cattell, K. Takahashi, S. J. Bame, and C. T. Russell, ISEE 1 and 2 Observations of magnetic flux ropes in the magnetotail: FTEs in the plasma sheet?, *Geophys. Res. Lett.*, *14*, 648, 1986.

Fairfield, D. H., et al., Geotail observations of substorm onset in the inner magnetotail, *J. Geophys. Res.*, *103*, 103, 1998.

Goldstein, H., On the field configuration in magnetic clouds, Solar Wind Five, *NASA Conf. Publ.*, *2280*, 731, 1983.

Goldstein, M. L., W. H. Matthaeus, and J. J. Ambrosiano, Acceleration of charged particles in magnetic reconnection: Solar flares, the magnetosphere, and solar wind, *Geophys. Res. Lett.*, *13*, 205, 1986.

Hesse, M., and M. G. Kivelson, The formation and structure of flux ropes in the magnetotail, in *New Perspectives on the Earth's Magnetosphere*, edited by A. Nishida, D. N. Baker, and S. W. H. Cowley, *Geophys. Monogr.*, vol. 105, pp. 139–152, AGU, Washington, D. C., 1998.

Hesse, M., J. Birn, D. N. Baker, and J. Slavin, MHD simulations of the transition of magnetic reconnection from closed to open field lines, *J. Geophys. Res.*, *101*, 10,805, 1996.

Hidalgo, M. A., C. Cid, A. F. Vinas, and J. Sequeiros, A non-force-free approach to the topology of magnetic clouds in the solar wind, *J. Geophys. Res.*, *106*, doi:10.1029/2001JA900100, in press, 2001.

Hones, E. W., Jr., Substorm processes in the magnetotail: Comments on "On hot tenuous plasma, fireballs, and boundary layers in the Earth's magnetotail" by L.A. Frank et al., *J. Geophys. Res.*, *82*, 5633, 1977.

Hones, E. W., Jr., D. N. Baker, S. J. Bame, W. C. Feldman, J. T. Gosling, D. J. McComas, R. D. Zwickl, J. A. Slavin, E. J. Smith, and B. T. Tsurutani, Structure of the magnetotail at 220 R_e and its response to geomagnetic activity, *Geophys. Res. Lett.*, *11*, 5, 1984.

Hoshino, M., Kinetic ion behavior in the magnetic reconnection region, in *New Perspectives on the Earth's Magnetosphere*, *Geophys. Monogr.*, vol. 105, edited by A. Nishida, D. N. Baker, and S. W. H. Cowley, pp. 153–166, AGU, Washington, D. C., 1998.

Hughes, W. J., and D. G. Sibeck, On the three dimensional structure of plasmoids, *Geophys. Res. Lett.*, *14*, 636, 1987.

Ieda, A., S. Machida, T. Mukai, Y. Saito, T. Yamamoto, A. Nishida, T. Terasawa, and S. Kokubun, Statistical analysis of plasmoid evolution with GEOTAIL observations, *J. Geophys. Res.*, *103*, 4435, 1998.

Ieda, A., D. H. Fairfield, T. Mukai, Y. Saito, S. Kokubun, K. Liou, C.-I. Meng, G. K. Parks, and M. J. Brittnacher, Plasmoid ejection and auroral brightenings, *J. Geophys. Res.*, *106*, 3845, 2001.

Khurana, K. K., M. G. Kivelson, L. A. Frank, and W. R. Paterson, Observations of magnetic flux ropes and associated currents in the Earth's magnetotail with the Galileo spacecraft, *Geophys. Res. Lett.*, *22*, 2087, 1995.

Kivelson, M. G., et al., The Galileo Earth encounter: Magnetometer and allied measurements, *J. Geophys. Res.*, *98*, 11,299, 1993.

Lee, L. C., A review of magnetic reconnection: MHD models, in *Physics of the Magnetopause*, *Geophys. Monogr.*, vol. 90, edited by P. Song, B. U. O. Sonnerup, and M. F. Thomsen, pp. 139–153, AGU, Washington, D. C., 1995.

Lepping, R. P., J. A. Jones, and L. F. Burlaga, Magnetic field structure of interplanetary magnetic clouds at 1 AU, *J. Geophys. Res.*, *95*, 11,957, 1990.

Lepping, R. P., D. H. Fairfield, J. Jones, L. A. Frank, W. R. Paterson, S. Kokubun, and T. Yamamoto, Cross-tail magnetic flux ropes as observed by the Geotail spacecraft, *Geophys. Res. Lett.*, *22*, 1193, 1995.

Lepping, R. P., J. A. Slavin, M. Hesse, J. A. Jones, and A. Szabo, Analysis of magnetotail flux ropes with strong core fields: ISEE 3 observations, *J. Geomagn. Geolectr.*, *48*, 589, 1996.

Lundquist, S., Magnetohydrostatic fields, *Ark. Fys.*, *2*, 361, 1950.

Machida, S., A. Ieda, T. Mukai, Y. Saito, and A. Nishida, Statistical visualization of the Earth's magnetotail during substorms by means of multidimensional superposed epoch analysis with Geotail data, *J. Geophys. Res.*, *105*, 25,291, 2000.

Marubashi, K., Structure of interplanetary magnetic clouds and their solar origins, *Adv. Space Res.*, *6*, 335, 1986.

Moldwin, M. B., and W. J. Hughes, Plasmoids as flux ropes, *J. Geophys. Res.*, *96*, 14,051, 1991.

Moldwin, M. B., and W. J. Hughes, On the formation and evolution of plasmoids: A survey of ISEE 3 geotail data, *J. Geophys. Res.*, *97*, 19,259, 1992.

Moldwin, M. B., and W. J. Hughes, Observations of earthward and tailward propagating flux rope plasmoids: Expanding the plasmoid model of geomagnetic substorms, *J. Geophys. Res.*, *99*, 184, 1994.

Moldwin, M. B., M. R. Collier, J. A. Slavin, and A. Szabo, On the origin of reverse polarity TCRs, *Geophys. Res. Lett.*, *28*, 1925, 2001.

Mukai, T., S. Machida, Y. Saito, M. Hirahara, T. Terasawa, N. Kaya, T. Obara, M. Ejiri, and A. Nishida, Low energy particle (LEP) experiment onboard the Geotail satellite, *J. Geomagn. Geolectr.*, *46*, 669, 1994.

Mukai, T., M. Fujimoto, M. Hoshino, S. Kokubun, S. Machida, K. Maezawa, A. Nishida, Y. Saito, T. Teresawa, and T. Yamamoto, Structure and kinetic properties of plasmoids and their boundary regions, *J. Geomagn. Geolectr.*, *48*, 541, 1996.

Mukai, T., T. Yamamoto, and S. Machida, Dynamics and kinetic properties of plasmoids and flux ropes: Geotail observations, in *New Perspectives on the Earth's Magnetosphere*, edited by A. Nishida, D. N. Baker, and S. W. H. Cowley, AGU, Washington, D. C., 1998.

Nagai, T., K. Takahashi, H. Kawano, T. Yamamoto, S. Kokubun, and A. Nishida, Initial Geotail survey of magnetic substorm signatures in the magnetotail, *Geophys. Res. Lett.*, *21*, 2991, 1994.

Nagai, T., M. Fujimoto, Y. Saito, S. Machida, T. Terasawa, R. Nakamura, T. Yamamoto, T. Mukai, A. Nishida, and S. Kokubun, Structure and Dynamics of magnetic reconnection for substorm onsets with GEOTAIL observations, *J. Geophys. Res.*, *103*, 4419, 1998a.

Nagai, T., M. Fujimoto, M. S. Nakamura, R. Nakamura, Y. Saito, S. Machida, T. Mukai, T. Yamamoto, A. Nishida, and S. Kokubun, A large southward magnetic field of −23.5 nT in the January 10, 1995 plasmoid, *J. Geophys. Res.*, *103*, 4441, 1998b.

Nagai, T., I. Shinohara, M. Fujimoto, M. Hoshino, Y. Saito, S. Machida, and T. Mukai, , *J. Geophys. Res.*, *106*, 25,929, 2001.

Nishida, A., T. Mukai, Y. Saito, T. Yamamoto, H. Hayakawa, K. Maezawa, S. Machida, T. Terasawa, S. Kokubun, and T. Nagai, Transition from slow flow to fast tailward flow in the distant plasma sheet, *Geophys. Res. Lett.*, *21*, 2939, 1994.

Nishida, A., T. Mukai, T. Yamamoto, S. Kokubun, and K. Maezawa, A unfied model of the magnetotail convection in geomagnetically quiet and active times, *J. Geophys. Res.*, *103*, 4409, 1998.

Owen, C. J., J. A. Slavin, I. G. Richardson, N. Murphy, and R. J. Hynds, Average motion, structure and orientation of the deep magnetotail determined from remote sensing of the edge of the plasma sheet boundary layer with E > 35 keV ions, *J. Geophys. Res.*, *100*, 185, 1995.

Priest, E. R., The equilibrium of magnetic flux ropes, *Geophys. Monogr.*, *58*, 1–22, 1990.

Richardson, I. G., S. W. H. Cowley, E. W. Hones Jr., and S. J. Bame, Plasmoid-associated energetic ion bursts in the deep geomagnetic tail: Properties of plasmoids and the post-plasmoid plasma sheet, *J. Geophys. Res.*, *92*, 9997, 1987.

Schindler, K., A theory of the substorm mechanism, *J. Geophys. Res.*, *79*, 2803, 1974.

Sergeev, V. A., R. C. Elphic, F. S. Mozer, A. Saint-Marc, and J. A. Sauvaud, A two-satellite study of nightside flux transfer events in the plasma sheet, *Planet. Space Sci.*, *40*, 1551, 1992.

Sergeev, V. A., V. Angelopoulos, J. T. Gosling, C. A. Cattell, and C. T. Russell, Detection of localized, plasma-deplete flux tubes or bubbles in the midtail plasma sheet, *J. Geophys. Res.*, *101*, 10,817, 1996.

Shirai, H., T. K. Takada, Y. Kamide, and T. Mukai, Enhancements of lobe ion density and velocity associated with plasmoids, *J. Geophys. Res.*, *106*, 29,935, 2001.

Sibeck, D. G., J. A. Slavin, E. J. Smith, and B. T. Tsurutani, Geomagnetotail twisting, in *Solar Wind-Magnetosphere Coupling*, edited by Y. Kamide and J. Slavin, pp. 731–738, Terra Sci., Tokyo, 1986.

Slavin, J. A., E. J. Smith, B. T. Tsurutani, D. G. Sibeck, H. J. Singer, D. N. Baker, J. T. Gosling, E. W. Hones, and F. L. Scarf, Substorm associated traveling compression regions in the distant tail: ISEE-3 Geotail observations, *Geophys. Res. Lett.*, *11*, 657, 1984.

Slavin, J. A., E. J. Smith, D. G. Sibeck, D. N. Baker, R. D. Zwickl, and S.-I. Akasofu, An ISEE-3 study of average and substorm conditions in the distant magnetotail, *J. Geophys. Res.*, *90*, 10,875, 1985.

Slavin, J. A., et al., CDAW-8 observations of plasmoid signatures in the geomagnetic tail: An assessment, *J. Geophys. Res.*, *94*, 15,153, 1989.

Slavin, J. A., M. F. Smith, E. L. Mazur, D. N. Baker, T. Iyemori, and E. W. Greenstadt, ISEE-3 observations of traveling compression regions in the Earth's magnetotail, *J. Geophys. Res.*, *98*, 15,425, 1993.

Slavin, J. A., C. J. Owen, M. M. Kuznetsova, and M. Hesse, ISEE 3 observations of plasmoids with flux rope magnetic topologies, *Geophys. Res. Lett.*, *22*, 2061, 1995.

Slavin, J. A., et al., ISTP observations of plasmoid ejection: IMP 8 and Geotail, *J. Geophys. Res.*, *103*, 119, 1998.

Slavin, J. A., et al., Dual spacecraft observations of lobe magnetic field perturbations before, during and after plasmoid release, *Geophys. Res. Lett.*, *26*, 2897, 1999.

Slavin, J. A., et al., Simultaneous observations of Earthward flow bursts and plasmoid ejection during magnetospheric substorms, *J. Geophys. Res.*, *107* (A4), 1106, doi:10.1029/2000JA003501, 2002.

D. H. Fairfield, J. Gjerloev, M. Hesse, R. P. Lepping, and J. A. Slavin, Laboratory for Extraterrestrial Physics, National Aeronautics and Space Administration/Goddard Space Flight Center, Greenbelt, MD 20771, USA. (james.a.slavin@gsfc.nasa.gov)

A. Ieda and T. Mukai, Institute of Space and Astronautical Science, 3-1-1 Yoshinodai, Sagamihara, Kanagawa 229, Japan.

M. B. Moldwin, ESS/Institute of Geophysics and Planetary Physics, University of California at Los Angeles, Los Angeles, CA, USA.

T. Nagai, Department of Earth and Planetary Sciences, Tokyo Institute of Technology, 2-12-1 Ookayama, Meguro, Tokyo, 152-8551, Japan.

C. J. Owen, Mullard Space Science Laboratory, University College London, Holmbury St. Mary, Dorking, Surrey RH5 6NT, UK.